Supercritical fluid coating of flavonoids on excipients enhances drug release and antioxidant activity

Hongling He,[a,∇] Yating Huang,[a,∇] Xiubing Zhang,[b,∇] Yanting Ouyang,[c,∇] Piaopiao Pan,[d] Yanling Lan,[a] Zicheng Zhong,[a] Lu Ping,[b] Tiejun Lu,[e] Zhenqiu Chen,[b,*] Lei Xing,[f,*] Qingguo Li,[a,*] Zhenwen Qiu,[b,*]

[a] School of Pharmaceutical Sciences, Guangzhou University of Chinese Medicine, Guangzhou 510006, P.R. China

[b] The First Affiliated Hospital, Guangzhou University of Chinese Medicine, Guangzhou 510405, P.R. China

[c] Shunde Hospital of Guangzhou University of Chinese Medicine, Foshan 528329, Guangdong, P.R. China

[d] Institute of Infection, Immunity and Inflammation, University of Glasgow, Glasgow G12 8QQ, UK

[e] Centre for Formulation Engineering, School of Chemical Engineering, University of Birmingham, Birmingham B15 2TT, UK

[f] Department of Chemical and Process Engineering, University of Surrey, Guildford GU2 7XH, UK

[∇] HH, YH, XZ, and YO contributed equally to this paper.

***Corresponding author**:

Zhenwen Qiu, The First Affiliated Hospital, Guangzhou University of Chinese Medicine, E-mail: qzhenwen@gzucm.edu.cn

Qingguo Li, School of Pharmaceutical Sciences, Guangzhou University of Chinese Medicine, 232 University City Ring Road East, Panyu District, Guangzhou 510006, China, E-mail: lqg8512@gzucm.edu.cn

Lei Xing, Department of Chemical and Process Engineering, Faculty of Engineering and Physical Sciences, University of Surrey, Guildford GU2 7XH, UK, E-mail: l.xing@surrey.ac.uk

Zhenqiu Chen, The First Affiliated Hospital, Guangzhou University of Chinese Medicine, E-mail: chenzhenqiu2012@126.com

Abstract: Supercritical anti-solvent fluidized bed (SAS-FB) technology can be applied to reduce particle size, prevent particle aggregation, and improve the dissolution and bioavailability of poorly soluble drugs. In this work, drug-loaded microparticles of three similar structures, the flavonoids luteolin (LUT), naringenin (NGR), and dihydromyricetin (DMY) were prepared using SAS-FB technology, to explore its effect on the coating of flavonoid particles. Operating temperature, pressure, solvent, and concentration of drug solution were investigated for their effects on the yield and dissolution of flavonoid particles. The results showed that temperature, pressure, carrier, and drug solution concentration have a large effect on yield. Within the study range, low supercritical CO_2 density at higher temperature and lower pressure, a larger surface area carrier, and moderate drug solution concentration led to a higher yield. The effect of the solvent on the yield of flavonoids is a result of multiple factors. Scanning electron microscopy (SEM) images showed that the drug-loaded particles prepared from different carriers and solvents have different precipitations pattern on the carrier surface, and their particle sizes were smaller than unprocessed particles and those prepared by the SAS process. Fluorescence microscopy (FM) results showed that the flavonoids were uniformly coated on the carrier. X-ray powder diffraction (XRPD) results showed that the crystalline morphology of SAS-FB particles remained unchanged after the SAS-FB process, although the diffraction peak intensity decreased. The cumulative dissolution of SAS-FB particles was more than four times faster in the first 5 minutes than that of the unprocessed flavonoids. The antioxidant activity of SAS-FB processed LUT, NGR and DMY was 1.89-3.78 times, 4.92-10.68 times and 0.99-2.57 times higher than that of the untreated flavonoids, respectively. The approach provides a reference for the application of SAS-FB technology in flavonoids.

Key words: Flavonoids, Naringenin, Dihydromyricetin, Luteolin, Supercritical anti-solvent fluidized

bed

1. Introduction

Flavonoids are a kind of polyphenol natural products widely existing in plants (Grotewold, 2006; Hendrich, 2006). Studies have shown that flavonoids a large number of which have antioxidant, anti-inflammatory and antiviral effects, and are potential drugs for the treatment of novel coronavirus pneumonia (COVID-19) (Alzaabi et al., 2022; Di Capua et al., 2017; Naeem et al., 2021; Ozkan et al., 2019; Panche et al., 2016). Lianhua Qingwen capsule (LQC) has been included in the diagnosis and treatment protocol for COVID-19 in China. Based on network pharmacology and molecule docking technology, scholars screened the active ingredients and targets of LQC, and found that several flavonoids, such as luteolin, naringenin, kaempferol, wogonin and quercetin, are potential effective active ingredients for anti-COVID-19 (Niu et al., 2021; Xia et al., 2020; Yan and Zou, 2021). Xiao et al. evaluated the binding force between DMY and SARS-CoV-2 M^{pro} by molecule docking and found that DMY maybe a hopeful therapeutic drug for antivirus and complications of COVID-19 (Xiao et al., 2021).

High oxidative stress characterizes viral pandemics and affects the antioxidant response (Trujillo-Mayol et al., 2021). One characteristic of viral infections is the tremendous production of reactive oxygen species (ROS) in both infected and healthy people during a health crisis (Beck and Levander, 1998; Wang et al., 2020). Too many ROS and oxidative stress products can further enhance the inflammatory response (McGarry et al., 2018). Flavonoids are able to scavenge free radicals directly by hydrogen atom donation (Prochazkova et al., 2011). Therefore, they are widely used in nutraceuticals, medicines and cosmetics (Fang et al., 2017). Flavonoids are highly lipophilic compounds that have poor solubility and low oral bioavailability and are sensitive to temperature, light, oxygen, and pH (Gujar and Wairkar, 2020; Nagula and Wairkar, 2019). Additionally, the particles have the advantage of higher intracellular uptake when the drug is in the submicron size range. Considerable efforts have been made to improve the dissolution and oral bioavailability of flavonoids by reducing

particle size by wet milling, high-pressure homogenization, spray drying, etc. (Gujar and Wairkar, 2020). However, these approaches commonly involve high energy consumption and high temperature during preparation, accompanied by changes in the flavonoid structure and antioxidant activities (Irina et al., 2020).

Supercritical antisolvent (SAS) technology effectively avoid light and heat by utilizing nonheating features and the low critical temperature of supercritical carbon dioxide (sc-CO_2). Therefore, the flavonoids prepared by SAS can also effectively maintain their activity. SAS has been reported to obtain particles with smaller sizes and more uniform distribution than other methods, which is attributed to the high diffusivity and lower viscosity of sc-CO_2 antisolvent (Padrela et al., 2018; Reverchon et al., 2007).

Hundreds of insoluble drugs have been prepared into micro- and nanoparticles by SAS, and their dissolution, antioxidation and bioavailability have been significantly improved (Abuzar et al., 2018; Ober, 2013). However, micro- and nanoparticles are prone to agglomeration due to their high surface energy, leading to adhesion and poor fluidity (Ober, 2013). Supercritical antisolvent fluidized bed (SAS-FB) technology can achieve simultaneous precipitation and coating in a single step to avoid agglomeration. This was applied to poorly soluble compounds to improve their dissolution and bioavailability. The most notable feature of SAS-FB is that it uses carrier particles as a fluidized bed and supercritical carbon dioxide fluid as fluidized gas. The drug particles precipitated from the SAS process are captured on the surface of the carrier instantly, without risks of agglomeration, and retain similar properties to the original nanoscale to microscale drug particles, thus increasing the solubility and flowability of the drug. Li et al. (Li et al., 2017) coated amorphous naringin nanoparticles on microcrystalline cellulose (MCC) and showed complete dissolution within 1 min. Therefore, SAS-FB offers an effective alternative to improve the release and bioavailability of poorly soluble flavonoids and their antioxidant activity can be maintained in solid dosage forms.

The SAS-FB process combines SAS and FB technology and is more complex than SAS

technology. It involves not only the influence of phase equilibrium and the mutual mass transfer between the organic solution and the supercritical fluid but also the influence of the carrier, fluidized bed process, mass transfer and kinetics of particle nucleation and growth (Montes et al., 2016). Moreover, the drug properties (polarity, lipophilicity, volatility, etc.) are affected by the chemical composition and greatly affect the solubility in supercritical fluids (Steckel et al., 1997), which has a significant influence on the SAS-FB process. It has been observed that the drug loading efficiency is closely related to the drug properties (Kalani and Yunus, 2011), for example, lipophilic drugs or CO_2-soluble drugs are difficult to precipitate (Yeo and Kiran, 2005). In this study, to explore flavonoid yield in the SAS-FB process and improve dissolution and antioxidant activity of flavonoid particles, we selected three flavonoids with potential to treat COVID-19: luteolin (LUT), naringenin (NRG), and dihydromyricetin (DMY). **Fig. 1** shows the structures and properties of the three flavonoids. The solubility of LUT, NRG and DMY in water are respectively 0.051mg/ml, NRG 0.046mg/ml, 0.2 mg/ml, and their relative bioavailability are 17.5%, 5.81% and 4.02%. We individually evaluated the impact of individual parameters on the drug yield and dissolution including temperature, pressure, carrier, drug solution concentration, and solvent, to provide a reference for the application of SAS-FB technology in flavonoids. The effects of the coated particles on the antioxidant activity of three flavonoids in vitro were investigated, which provided a new perspective for the discovery of potential drugs for COVID-19.

2. Materials and methods

2.1. Materials

Naringenin standard (98%), luteolin standard and dihydromyricetin standard were purchased from Chengdu AIfa Biotechnology Co., Ltd. (Chengdu, China); naringenin (98%) and luteolin (96%) were purchased from Yunnan Lilian Co., Ltd. (Yunnan, China); dihydromyricetin (98%) was purchased from Topscience Co., Ltd. (Shanghai, China); acetonitrile (HPLC grade), methanol (HPLC grade) and ethanol (A.R. grade) were purchased from Tianjin Tianli Chemical Reagent Co., Ltd.

(Tianjin, China); carbon dioxide (99.8 v/v%) was purchased from Yingxin Gas Co. Ltd. (Guangzhou, China). Microcrystalline cellulose (MCC) with particle size ranges of 400~600 μm and sucrose with a particle size range of 300~400 μm were purchased from Haining Weijing Pharmaceutical Excipients Technology Development Co. Ltd. (Hangzhou, China). Lactose T70, with a particle size range of 150~250 μm, was imported from Beauty Agents Co. Ltd., (Germany); 1,1-diphenyl-2-dinitrophenylhydrazine (DPPH) was purchased from Guangzhou Suchengyue Co., Ltd. (Guangzhou, China).

2.2. The silica gel thin layer

The polarities of flavonoids were determined by silica gel thin layer (**Fig. 1**). LUT, NRG and DMY were dissolved in methanol to prepare a 1.0 mg/mL solution. The solution was then spotted on a silica gel G plate, developed with a developing solvent (toluene-methyl formate-formic acid (5:4:1)) and air-dried. The samples were sprayed with a chromogenic agent (1% aluminum trichloride solution) and placed in an oven at 105 °C for 2 min. The samples were removed and observed under 254 nm and fluorescent light.

2.3. Ultrahigh-performance liquid chromatography (UHPLC)

UHPLC (Ultimate 3000, Thermo Scientific, USA) was used to quantify the LUT, NRG, and DMY in the samples. The analytical column used was a C18 column (Diamonsil C18, 250 × 4.6 mm, 5 μm, Dikma Technologies). The sampling volume was 10 μL at a flow rate of 1 mL/min in isocratic mode.

For LUT the mobile phase was composed of filtered and degassed acetonitrile and 0.4% acetic acid aqueous solution at a ratio of 58:42. The detection wavelength was set at 350 nm.

For NRG the mobile phase was composed of filtered and degassed acetonitrile and water at a ratio of 90:10. The detection wavelength was set at 288 nm.

For DMY the mobile phase was composed of filtered and degassed acetonitrile and 0.1% phosphoric acid aqueous solution at a ratio of 40:60. The detection wavelength was set at 290 nm.

2.4. Drug yield

The total amount of drug present in the formulations was determined by dissolving the appropriate sample in acetonitrile, a solvent in which flavonoids are soluble. The flavonoid content was then determined by UHPLC. The yield of the flavonoids on the carrier was then estimated by Eq. (1) - (2):

$$m_p = C \times m_s \tag{1}$$

$$drug\ yield\ (\%) = \frac{m_p}{m_i} \times 100\% \tag{2}$$

where C is the measured mass of the drug in the SAS-FB sample, m_s is the total mass of the SAS-FB samples composed of coated drugs and carriers in one experiment, m_p is the mass of the drug precipitated, and m_i is the mass of the drug introduced during the SAS-FB process.

3. Particle preparation by SAS-FB

A detailed description of the SAS-FB process has been reported previously (Li et al., 2017). In brief, a certain mass (2 g) of carriers to be coated (host particles) was first loaded into the fluidized bed holder. Two layers of quantitative filter papers (Whatman, 1-3 μm) were placed on the top of the fluidized bed holder to prevent particles being blown out. Then, the bed holder was placed inside the 500 mL high-pressure vessel (HPV). After that, CO_2 was slowly (lower than the minimum fluidization flow rate) introduced into the HPV through the bottom of the fluidized bed until the desired pressure was reached and then the gas flow rate was increased to fluidize the carrier particles until a constant CO_2 flow was reached by adjusting the outlet valve. The upward movement of sc-CO_2 through the gas distributor promoted the fluidization of the host particles. When the pressure, temperature and CO_2 flow rate were stable, pure solvent was injected into the bed at the same flow rate as the experimentally set value (0.5 mL/min) to build up a quasi-steady concentration of the solvent in CO_2. Then the drug solution was delivered sequentially into the fluidized bed (0.5 mL/min), allowing flavonoid precipitation (guest particles) onto host particles. After the designed drug solution was injected, enough pure solvent was used to purge the pipelines at the same flow rate while keeping the CO_2 flow unchanged. Then, the solvent pump, was stopped, and CO_2 was flowed for 15 min to wash. Finally, the system was slowly depressurized, and the sample was collected for further analysis. The mass of

drug used in each run was kept constant at 50 mg for all experiments, and all other investigated experimental parameters are listed in **Table 1**.

4. Analyses

4.1. Scanning electron microscopy (SEM)

Samples were deposited onto double-sided tape and sputtered with platinum for 200 s at a pressure of 0.5 mbar before the analysis. SEM images were taken using a Sigma 500 scanning electron microscope (ZEISS, Germany). The imaging was performed at 10 kV and 10 mA. ImageJ analysis software was used to measure aspect ratio and roundness.

4.2. Fluorescence microscopy (FM)

Fluorescence microscopy was performed the produced powders using an Olympus fluorescence microscope (Olympus, BX53, Japan) to observe and analyze the distribution of the coating on the carrier. Violet radiation (λ_{max} 372 nm) was used for absorbing, and blue fluorescence (λ_{max} 456 nm) was emitted.

4.3. X-ray powder diffraction (XRPD)

To investigate the crystallinity of the samples, their XRPD patterns were recorded on an X-ray powder diffraction system (Ultima IV, Japan). Powder samples were examined with a beam angle from 5° to 45° and a step size of 0.05°. The generator tension (voltage) and generator current were maintained at 40 kV and 20 mA, respectively.

4.4. Fourier transform infrared spectroscopy (FT-IR)

The comparison of chemical functionalities between the processed and unprocessed flavonoids was performed using a Fourier transform infrared (FT-IR) spectrophotometer (Spectrum 100 FT-IR, PerkinElmer, USA) in the range of 400-4000 cm^{-1}. Approximately 5 mg of sample and 100 mg of dry KBr were uniformly blended in an agate die and pressed into a translucent disc. The spectra were composed of 64 scans with a resolution of 4 cm^{-1} at room temperature.

4.5. In vitro dissolution studies

The dissolution test was performed using a USP paddle dissolution apparatus (ZRS-8G dissolution tester, Tianda Tianfa Technology Co. Ltd, Tianjin, China) under sink conditions at 37 ± 0.5 °C. One milliliter aliquots were taken at the sampling time and immediately replaced by 1 mL dissolution medium. All solutions were filtered through a 0.22 μm nylon membrane before UHPLC analysis. The results are the average of triplicate test values for each point.

LUT samples used 500 mL 0.1% SDS aqueous solution as the dissolution medium, and the stirring speed was set at 100 rpm. For NRG, 1000 mL of distilled water was used as the dissolution medium, and the stirring speed was set at 50 rpm. All samples used the equivalent of 5 mg of bulk drug, and 1 mL was taken at 5, 10, 20, 30, 45 and 60 min. An appropriate amount of LUT and NRG filtrate was added to an equal volume of acetonitrile and vortexed for 2 min for UHPLC analysis.

One thousand milliliters of distilled water was used as the dissolution medium for DMY samples (equivalent to 3 mg DMY), and the stirring speed was set at 50 rpm. One milliliter was taken at 1, 3, 5, 10, 15, and 30 min and the same procedure was followed as the other two samples.

4.6. Measurement of DPPH radical-scavenging activity

Three samples were accurately weighed, each containing equivalent amounts of drug (10 mg), and separately added into three vials containing 20 mL deionized water. The samples were shaker in shaker for 20 min. Then, each sample was centrifuged for 15 min at 8000 rpm. The obtained supernatant was diluted into different concentration samples, namely 1.0, 3.1, 6.2, 12.5, 25.0 and 50.0 μg/mL (calculated by the initial suspension). Each sample (100 μL) was mixed with 100 μL of ethanol DPPH solution (0.1 mmol/L) in numbered 96-well plates. After shaking evenly, the 96-well plates were placed at room temperature in the dark. After 30 min, the absorbance of the samples was measured at 517 nm. The experiment was repeated three times and the average value was taken. The ability to scavenge DPPH radicals was calculated by Eq. (3):

$$DPPH\ radical - scavenging\ rate\ (\%) = \frac{Ac-Ai}{Ac} \times 100 \quad (3)$$

where Ac is the absorbance of the control and Ai is the absorbance of the sample.

5. Results and discussion

5.1 Influence of various parameters

The yields of flavonoids of the SAS-FB process under different conditions are shown in **Table 2**.

5.1.1 Temperature and pressure

SAS-FB was investigated at temperatures ranging from 37 to 45 ºC and pressures ranging from 80 to 120 bar (**Table 2,** Exp. 1,2.3 and 2,4,5). The yield improves with increasing temperature from 37 to 45 °C (at P = 80 bar,) and decreasing pressure from 120 to 80 bar (at T = 40 °C). Other conditions remained constant (**Fig. 2a**).

The density of sc-CO_2 depends on the temperature and pressure of the operating conditions (Kalani and Yunus, 2011). It affects the mass transfer between the organic solvent and sc-CO_2 as well as the solubility of the drug in sc-CO_2 (Duarte et al., 2009; Li et al., 2008). This in turn varies the drug yield and particle size.

Analysis of drug yield and sc-CO_2 density showed a strong negative association (**Table 3**); that is, the yield increased with decreasing density of sc-CO_2 (**Fig. 2b**). When the density of sc-CO_2 increases from 0.241 to 0.718 g/cm^3, the yield of all three flavonoids decreases: LUT from 39.4% to 24.2%, NRG from 57.7% to 35.1%, and DMY from 59.7% to 20.5%. They all achieved the highest yield at 80 bar and 45 °C. Referring to “Solubility in Supercritical Carbon Dioxide” (Gupta and Shim, 2006), this temperature and pressure is where the sc-CO_2 density within the working range of that work. The increasing density of sc-CO_2 represents a decrease in the intermolecular mean distance of the molecules and an increase in specific interactions between the solute and solvent, leading to a higher solubility of the drug in sc-CO_2 (Xia et al., 2012). As a result, higher yields are achieved at lower densities (Duarte et al., 2009; Montes et al., 2016).

In addition, it is worth noting that LUT, NRG, and DMY are structurally similar, but with different numbers of hydroxyl groups. The LUT has a double bond between positions 2 and 3. As shown in **Fig. 2b**, the yields of NRG and DMY exhibit a significant upward trend with decreasing sc-CO_2 density.

The density of sc-CO_2 decreases from 0.718 to 0.241. The resulting yield of NRG increases by approximately 22% and the yield of DMY increases by approximately 39%, especially in the range of 0.241 to 0.355 g/cm^3, where the yield varies significantly. The variation in LUT yield with the density of sc-CO_2 is relatively gentle, and an increase of approximately 15% is obtained. This result indicates that NRG and DMY yields are more sensitive to sc-CO_2 density than LUT.

5.1.2 Carrier type

Three carriers, MCC, sucrose, and lactose, were investigated in this work. The yield of three flavonoids for each carrier is shown in **Table 2** (Exp. 2, 6 and 7). On carriers MCC, sucrose, and lactose, the yields of LUT are 30.0, 37.1, and 38.0%, respectively. The yields of NRG are 13.3, 36.8, and 45.9% and the yields of DMY are 16.1, 42.7, and 48.1%, respectively. The three flavonoids had the highest yields when lactose was used as the carrier (**Fig. 3a**).

Saint-Lorant et al. (2007) reported that the lower the sphericity of the carrier particles, the more significant the adhesion of the drug and carrier. The lactose T70 used in our study has a "blackberry" structure with a typical rough and porous surface. The MCC and sucrose have relatively smooth surfaces and perfect spherical shapes, especially MCC (**Fig. 4**), which is also confirmed by the measured aspect ratio and roundness of these three carriers using ImageJ software (**Fig. S1** in **SI)**. In addition, the distribution of flavonoids was observed in the fluorescence images (**Fig. 6** and **Fig. S2** in **SI**). MCC exhibits irregular spot-like fluorescence, suggesting that the drug coated on the surface was unequal and had small coverage, while stronger and more uniform fluorescence responses were found on sucrose and lactose. The three flavonoids had the highest yields on lactose, the least spherical carrier. This indicates that the surface roughness and sphericity of carriers affect the contact areas of the particle-to-particle surface (Kaialy, 2016), which may affect its ability to capture drug microparticles.

It was also found that flavonoids exhibit different morphologies on different carriers (**Fig. 4**). The morphology of LUT precipitates is flaky on lactose, irregular clastic on sucrose (**Fig. 4d** and **e**), and irregular needle-like and sheet-like on MCC **(Fig. 4d, e, f**). NRG appears as rectangular flakes on

lactose (**Fig. 4g**), uniform short columns on sucrose (**Fig. 4h**), and large cluster crystals on MCC (**Fig. 4i**). DMY shows similar short columnar crystals on lactose and sucrose but forms a "cobweb" structure on MCC (**Fig. 4 j, k, l**). This may be because the carrier particle shape affects the extent of inter-particle surface contact, and therefore, the magnitude of short-range van der Waal' S forces (Saint-Lorant et al., 2007), resulting in the different adhesion morphologies of the precipitated drug particles.

5.1.3. Concentration of drug solution

The concentration of the drug solution is related to the yield of the SAS process (Kim et al., 2012; Sui et al., 2012). The precipitation of the drugs from acetone at various drug concentrations in the range from 1.0 to 5.0 mg/mL (T = 40 °C, P = 80 bar, f=0.5 ml/min, f_{CO2}=32 g/min) was performed to investigate the effect of the concentration on the drug yield of the SAS-FB process. **Fig. 3b** shows the variation trend of the yield of the three flavonoids with different solution concentrations. The yield of flavonoids appears to be the maximum at a certain drug concentration. In general, the yield of flavonoids first increased and then decreased.

Increasing the drug solution concentration effectively increases the supersaturation of the liquid under the prevailing conditions (Sinha et al., 2013; Sui et al., 2012), which could increase the yield of flavonoids. After the peak value, the drug yield decreases when the drug concentration further increases to 5.0 mg/mL. This is probably a result of an increase in the viscosity of the drug solution at elevated concentrations, resulting in poor species diffusion between sc-CO_2 and acetone and nonuniform supersaturation (Matos et al., 2018; Rosa et al., 2020). Additionally, the more concentrated the solution is, the faster the solute precipitation process is. As a result, there is not enough time to distribute the solute over the carrier surface, which can explain the decrease in drug yield in this experiment when the drug concentration is further increased (Martín et al., 2015).

5.1.4. Solvent

The solvent has a large effect on the yield of the precipitated drug due to different solvent-solute interactions during SAS (Barrett et al., 2008; Djerafi et al., 2017). Studies have confirmed that, for

flavonoids, using a mixture of a “good solvent” (such as acetone, methanol, ethanol) and a “poor solvent” (such as DCM) in SAS allow the production of smaller particles, which is conducive to dissolution (De Marco et al., 2015; Miao et al., 2018). For solvents, this experiment evaluated methanol, ethanol, acetone, and acetone-dichloromethane (ACE-DCM, 55:45) mixtures (T = 40 °C, P = 80 bar, C_{drug} = 2.5 mg/mL, f = 0.5 mL/min, f_{CO2} = 23 g/min). As **Fig. 3** shows, the maximum yield of DMY was obtained when methanol was used as the solvent (62.4%). The yield of NRG was the highest when using acetone-dichloromethane (62.3%) as the solvent, and the yield of LUT was the highest when using acetone (38.0%) as the solvent.

The effect of solvent on the yield of flavonoids depends on the physicochemical properties of solvent and flavonoids as well as the solubility of drugs in the solvent and in sc-CO_2. Different solvents have different physical and chemical properties, such as dielectric constant, viscosity, density, and surface tension, which can influence the drug-solvent interaction and drug deposition.

The dielectric constant reflects the polarity of the solvent. The dielectric constants of the four solvents are presented here in descending order: methanol > ethanol > acetone > dichloromethane. The polarities of the three flavonoids were determined by the silica gel thin layer test (**Fig. 1d)**, and the results were as follows: NRG < LUT < DMY. From the molecular structure, DMY has more hydroxyl groups and larger polarity. According to the theory of "poor solvent", solvents with lower solubility should be selected because they are conducive to drug deposition in sc-CO_2, but the experiments have shown the opposite. The yield of DMY was highest in methanol (62.3%) which has the greatest polarity, and lowest in the ACE-DCM mixture (34.0%), which has the lowest polarity. NRG has the lowest polarity of the three flavonoids; however, it has the highest yield in the ACE-DCM mixture (62.3%) with the lowest polarity, and the lowest yield (35%) in methanol with the highest polarity. In addition, the yield of intermediate polarity LUT in the intermediate polarity solvent ethanol was the highest (37.4%). This result is consistent with the NRG and DMY. From the above results, it can be determined that a particular choice of solvent is beneficial to the coating of a certain flavonoid. A drug with high

polarity benefits from a solvent with high polarity, and a flavonoid with low polarity benefits from a solvent with lower polarity. However, the yield of flavonoids is the result of many factors, possibly also related to viscosity, density, and surface tension. The Weber number ($We=\rho v^2 d/\sigma$) is a dimensionless number used for analyses of fluid flow where the surface tension influences the flow. In the spray process, the Weber number is the ratio of the deforming external pressure forces and the reforming surface tension forces experienced by a liquid droplet encountering flowing air. When the Weber number increases, the initial droplet size decreases and smaller solid particles are produced, which may affect the particle yield.

Therefore, the effect of the solvent on the yield of flavonoids are a comprehensive result, and the analysis and inference of single parameter cannot reflect the influence of solvent on yield completely and accurately. Due to technical limitations, the current experimental results cannot fully determine the influence of solvents on the yield, but they can be used to determine which solvent is more suitable for a specific flavonoid coating.

The choice of solvents is also known to affect the morphology of precipitates in the SAS process (Liu et al., 2013; Varughese et al., 2010). The effect of solvent on the morphology of flavonoid particles was studied and can be observed in **Fig. S3** in **SI**. When methanol, ethanol and acetone as solvents, the morphology of the LUT particles was flake-like, leaf-like crystal, and flocculent-like, respectively (**Fig. S3 a, b, c**); the morphology of NRG was in strips of different lengths, thin columnar, and columnar, respectively (**Fig. S3 d, e, f**), exhibiting more of a difference in thickness and length. The morphology of the DMY was that of short rod-shaped, needle-like, and irregular granular crystals, respectively (**Fig. S3 g, h, i**). These results indicate that different solvents used in the SAS-FB process have an effect on the morphology of flavonoids. This can be attributed to the different CO_2-solvent-solute miscibility limits, densities, viscosities, solvent strengths, and solvent-solute interactions. Simultaneously, an increase in the solvent dielectric constant decreases the molecular energy and increases the dipole moment (Sinha et al., 2013). The change in the dipole moment alters the molecular

conformation and may also influence the direction of structurally-dominant periodic bond chains of molecules during crystal growth, resulting in different crystal morphologies (Rossmann et al., 2014; Sinha et al., 2013).

In summary, low supercritical CO_2 density at high temperature and low pressure, larger surface area of carriers, and moderate drug solution concentration led to a higher yield of all three studied flavonoids. The effect of the solvent on the yield of flavonoids is a result of multiple factors (see **Fig. S4** in SI).

5.2. Particle Characterization

The coating of the drug on lactose (SAS-FB samples) was characterized by fluorescence microscopy (FM). The crystallinities of the unprocessed drug, SAS, and SAS-FB samples were measured by X-ray powder diffraction (XRPD). The interaction between lactose and the drug was studied by Fourier transform infrared spectroscopy (FT-IR).

The spontaneous fluorescence properties of LUT, NRG, and DMY made them suitable for FM analysis to visualize the flavonoid coating on lactose. The FM results are shown in **Fig. 6**. It is clear that when LUT is precipitated on the lactose surface, the blue fluorescence of lactose is covered by a stronger orange fluorescence of LUT **(Fig. 6d)**. The NRG-coated lactose **Fig. 6e** shows yellowish-green NRG fluorescence over the blue lactose fluorescence, while the yellow fluorescence of DMY (**Fig. 6c**) completely covered the blue lactose fluorescence in **Fig. 6f** for the SAS-FB sample of DMY-coated lactose. This suggests that the flavonoids were successfully coated on the surface of the carrier by the SAS-FB process.

The XRPD patterns of the three unprocessed flavonoids, lactose SAS samples, and lactose SAS-FB samples are shown in **Fig. 7**. The XRPD patterns of other uncoated carriers (sucrose and MCC) and corresponding SAS-FB samples of the three flavonoids are shown in **Fig. S8** in **SI**. Uncoated carriers processed under condition 2 in Table 2 shows the crystalline diffraction peaks, which confirm carrier no amorphous content after processed in sc-CO_2. The presence of better-defined peaks in the

X-ray spectrum indicates that all three flavonoids (API) are crystalline materials. **Fig. 7a** shows that at 10.30°, 14.36°, 15.94°, 20.36°, 22.18°, 22.76°, 25.6°, 26.4°, 27.28°, and 28.2°, unprocessed LUT shows significant crystallization diffraction peaks (**Fig. 7a**). However, the XRPD pattern of SAS particles shows a change in peak angle and a new peak appearance at 7.5°. Differences in displacement and the appearance/disappearance of peaks represent the polymorphic forms of the compounds, as they are formed in different patterns of XRPD. The results indicate that the crystal structure of the LUT particles changed (dos Santos et al., 2022). **Fig. 7b, c** shows that after SAS processing, the peak intensity of LUT and DMY prominently decreased, while NRG still had high crystallinity. This means that there was a reduction in the crystallinity of SAS samples compared with unprocessed DMY. These data make it possible to infer that, although the drug undergoes a size change, significant changes in the crystal arrangement are not present (Cui et al., 2019). The limited variation of the XRPD patterns of the SAS-FB samples and carriers (MCC, lactose, sucrose), as shown in **Fig. 7** and **Fig. S8**, can be explained by the low drug loading. In other words, the XRPD patterns of the SAS-FB samples were highly similar to that of the blank carrier and there were almost no observed crystallization peaks of the drug. However, according to the SEM results, the SAS and SAS-FB samples of the three flavonoids have certain crystal morphology characteristics, which can be seen in **Fig. 4** and **Fig. 5**. Therefore, it is believed that the flavonoids prepared through SAS-FB process is still crystalline, and the improvement of dissolution is more attributable to the reduction of flavonoids particle size.

To explore the possible intermolecular interaction between flavonoids and the carrier after the SAS-FB process and evaluate the different functional groups present in the three flavonoid structures, blank excipients, unprocessed flavonoid drug, and SAS-FB-coated particles were characterized by FT-IR spectroscopy in the wavelength range of 4000 to 400 cm^{-1} (**Fig. 8)**. It is noted that the unprocessed LUT, NRG, and DMY displayed the same functional groups as the SAS samples, suggesting that the SAS process does not influence the structure of the flavonoids. Moreover, the spectrogram of the SAS-FB samples showed high similarity to the pure lactose, indicating that there is no chemical bond

interaction between the two compounds.

5.3. Dissolution profiles of processed and unprocessed flavonoids

The flavonoid dissolution profiles of the API, SAS, and SAS-FB samples are shown in **Fig. 9**. The samples processed by SAS-FB show significantly faster dissolution than unprocessed particles and faster dissolution than SAS samples. The LUT samples prepared by SAS-FB dissolved approximately 75% at 60 minutes, which is approximately four times higher than that of the unprocessed LUT (**Fig. 9a)**. For NRG microparticles prepared by SAS-FB, the dissolution reaches 90% at 60 minutes, which is approximately four times higher than that of the unprocessed microparticles (**Fig. 9b)**. The SAS-FB sample of DMY reached more than 80% dissolution at 1 min, which is 5.52 times faster than unprocessed DMY (**Fig. 9c)**.

In addition, the dissolution profile of all the samples prepared under different processing conditions were investigated (see **Fig. S5 - S7** in SI). The change of temperature and pressure has limited influence on the dissolution profiles of the three flavonoids. However, LUT and NRG show different dissolution profiles when different carriers are used. When MCC is implemented as carrier, the dissolution of three drugs is slower than that of lactose and sucrose, which can be explained by the hydrophilicity of the carrier. Since lactose and sucrose can dissolve in water rapidly, drug particles could disperse well in the aqueous phase, leading to a faster dissolution owing to the improved solid-liquid interfacial area. The dissolution profiles of LUT and NRG SAS-FB samples prepared with different solvents and drug concentrations are different. Moreover, the dissolution of DMY SAS-FB samples with higher water solubility is less affected by the processing conditions.

One of the factors affecting the dissolution rate is described by the Noyes-Whitney equation which states that the dissolution rate of a drug is directly proportional to the solid-liquid interfacial area, so the accelerated dissolution rate of microparticles can be attributed to the reduction in particle size (Savjani et al., 2012). It can be seen from the SEM images that the particle size of the three flavonoid microparticles on the excipient by SAS-FB was smaller than that on the API (**Fig. 4** and **Fig.**

5).

Moreover, the dissolution ratio of SAS-FB LUT samples in the first 5 minutes is 4.12 times higher than that of SAS LUT samples (**Fig. 9**). SEM shows that drug particles prepared by SAS are fluffy and much smaller than the bulk drug, but they are prone to aggregation (**Fig. 5**), which limits the dissolution of the drug (Ober et al., 2013). However, during the SAS-FB process, the lactose carrier in the fluidized bed captures most of the nuclei, thus limiting their further growth (Chen et al., 2020). The experimental results show that the aggregation of particles is effectively mitigated by the SAS-FB process and that the anti-aggregation effect further improves the dissolution rate of the drug.

In addition, although the particle size of SAS microspheres was smaller than that of the bulk drug (**Fig. 5**), **Fig. 9** shows the dissolution profile of the NRG samples, and the dissolution rate of the SAS sample basically coincides with that of the unprocessed NRG. The XRPD result shows that the crystallinity of the SAS-processed NRG is still strong (**Fig. 7b)**. This suggests that the dissolution rate is also related to crystallinity. The dissolution rates of all three particles prepared through SAS-FB are significantly improved. Especially in the first 10 minutes, the cumulative dissolution reaches > 60%, which is superior to the raw API that only dissolves 1-20%. Process parameters has little effect on the dissolution rate of all the particles, expect the remarkable influence of carriers on the dissolution of NRG. The dissolution rates of the SAS-FB prepared particles are different owing to the difference in the solubility of drugs in water. In particular, DMY rapidly dissolves > 80% in 1 minutes, which is much faster than LUT and NRG. Obvious difference in dissolution rates is also found among the flavonoid particles prepared by SAS, with the least variation of NRG samples.

5.4. DPPH radical-scavenging activity measurement

Flavonoids have strong antioxidant activity (Ross and Kasum, 2002). The antioxidant activity of flavonoids is generally correlated with their potential to their anti-inflammatory effects. In general, the radical scavenging rate of DPPH indicates antioxidant activity of the drug (Sheng et al., 2020). To verify the effect of the SAS-FB process on the antioxidant activity of flavonoids, this work investigated

the inhibition degree of flavonoids on free radicals by DPPH in vitro. **Fig. 10** presents the antioxidant capacity at different concentrations of the three flavonoid drugs.

The samples prepared through SAS-FB showed higher antioxidant activity than the unprocessed drug. The antioxidant activity of SAS-FB LUT is 1.89-3.78 times higher than that of the unprocessed drug. The SAS-FB-processed NRG is 4.92-10.68 times higher and the SAS-FB-processed DMY is 0.99~2.57 times higher than their unprocessed drug. This fact is consistent with the particle size shown in the SEM images (**Fig. 4** and **Fig. 5**). In other words, samples prepared by SAS-FB had smaller particle sizes than those prepared by API. The results show that the antioxidant activity of flavonoid particles was significantly increased due to the greater improvement in dissolution (smaller particle size) of flavonoids. The flavonoids prepared by SAS-FB technology have small particle size and faster dissolution, which increases the content of flavonoids in water. Flavonoids are able to scavenge free radicals directly by proton donation, which is represented by the following equation (Prochazkova et al., 2011).

$$\text{Fl-OH} + \text{R}\bullet \rightarrow \text{Fl-O}\bullet + \text{RH} \quad (4)$$

where R• is a free radical and Fl-O• is a flavonoid radical.

Antioxidants have the ability to provide H^+ or e^- to DPPH and convert DPPH into DPPH-H. Therefore, the antioxidant activity of antioxidants is mainly related to the contribution ability of e^- or H^+ (Alshehri et al., 2020). As a result, for the studied flavonoids, the particles prepared though SAS-FB technology can improve the antioxidant activity of the target compounds. The antioxidant activities of all three particles prepared by SAS-FB are improved. However, due to the difference in the dissolution rate and the number of hydroxyl groups in the molecular structures, the three flavonoid particles exhibit different antioxidant activities. For example, the DMY particles prepared through SAS-FB process at a low concentration, e.g., 1 μg/ml, show stronger antioxidation activity than LUT and NRG particles and the API, which can be explained by the faster dissolution rate and larger number of hydroxyl groups of DMY particles.

6. Conclusion

Drug-loaded microparticles of three flavonoids were prepared by SAS-FB technology. It was found that the lower the density of process CO_2 with high temperature and low pressure, the higher the drug yield. The effect of solvent on drug yield could not be fully determined, but we can determine the optimal solvent for selected drugs in their respective SAS-FB processes. Moreover, the larger the surface area and roughness of the carrier are, the higher the yield. The morphology of flavonoid crystals is carrier-dependent and solvent-dependent.

This study explored SAS-FB preparation of three insoluble flavonoids. Similar trends were found with respect to the effect of CO_2 density, carrier, and drug concentration on drug yield in the SAS-FB process for the three flavonoids with similar structures. The solubility of the three flavonoids in water and organic solvent is different due to the difference in hydroxyl groups, which leads to different influence of organic solvent on the yield, dissolution rate and antioxidant activity of the prepared particles. It was confirmed that SAS-FB can improve the dissolution and biological activity of insoluble flavonoids, which provides a new perspective for the discovery of potential drugs.

Acknowledgement

The authors acknowledge the support from the competitive talent project of Foshan, Guangdong province, China (FSRC20220004).

Reference

S. M. Abuzar, S.-M. Hyun, J.-H. Kim, H. J. Park, M.-S. Kim, J.-S. Park and S.-J. Hwang, 2018. Enhancing the solubility and bioavailability of poorly water-soluble drugs using supercritical antisolvent (SAS) process. International journal of pharmaceutics 538, 1-13.

S. Alshehri, S. S. Imam, M. A. Altamimi, A. Hussain, F. Shakeel, E. Elzayat, K. Mohsin, M. Ibrahim and F. Alanazi, 2020. Enhanced Dissolution of Luteolin by Solid Dispersion Prepared by Different Methods: Physicochemical Characterization and Antioxidant Activity. Acs Omega 5, 6461-6471.

M. M. Alzaabi, R. Hamdy, N. S. Ashmawy, A. M. Hamoda, F. Alkhayat, N. N. Khademi, S. M. A. Al Joud, A. A. El-Keblawy and S. S. M. Soliman, 2022. Flavonoids are promising safe therapy against COVID-19. Phytochemistry Reviews 21, 291-312.

A. M. Barrett, F. Dehghani and N. R. Foster, 2008. Increasing the dissolution rate of itraconazole processed by gas antisolvent techniques using polyethylene glycol as a carrier. Pharmaceutical research 25, 1274-1289.

M. A. Beck and O. A. Levander, 1998. Dietary oxidative stress and the potentiation of viral infection. Annual Review of Nutrition 18, 93-116.

T. Chen, L. Liu, L. Zhang, T. Lu, R. L. Matos, C. Jiang, Y. Lin, T. Yuan, Z. Ma and H. He, 2020. Optimization of the supercritical fluidized bed process for sirolimus coating and drug release. International Journal of Pharmaceutics 589, 119809.

W. Cui, Z. He, Y. Zhang, Q. Fan and N. Feng, 2019. Naringenin cocrystals prepared by solution crystallization method for improving bioavailability and anti-hyperlipidemia effects. AAPS PharmSciTech 20, 1-12.

I. De Marco, M. Rossmann, V. Prosapio, E. Reverchon and A. Braeuer, 2015. Control of particle size, at micrometric and nanometric range, using supercritical antisolvent precipitation from solvent mixtures: Application to PVP. Chemical Engineering Journal 273, 344-352.

A. Di Capua, R. Adami and E. Reverchon, 2017. Production of luteolin/biopolymer microspheres by supercritical assisted atomization. Industrial Engineering Chemistry Research 56, 4334-4340.

R. Djerafi, A. Swanepoel, C. Crampon, L. Kalombo, P. Labuschagne, E. Badens and Y. Masmoudi, 2017. Supercritical antisolvent co-precipitation of rifampicin and ethyl cellulose. European Journal of Pharmaceutical Sciences 102, 161-171.

A. E. dos Santos, C. Dal Magro, L. S. de Britto, G. P. S. Aguiar, J. V. de Oliveira and M. Lanza, 2022. Micronization of luteolin using supercritical carbon dioxide: Characterization of particles and biological activity in vitro. The Journal of Supercritical Fluids 181, 105471.

A. R. C. Duarte, J. F. Mano and R. L. Reis, 2009. Preparation of chitosan scaffolds loaded with dexamethasone for tissue engineering applications using supercritical fluid technology. European Polymer Journal 45, 141-148.

Y. Fang, W. Cao, M. Xia, S. Pan and X. Xu, 2017. Study of Structure and Permeability Relationship of Flavonoids in Caco-2 Cells Nutrients 9, 1-15.

E. Grotewold, 2006. The science of flavonoids. Springer.

K. Gujar and S. Wairkar, 2020. Nanocrystal technology for improving therapeutic efficacy of flavonoids. Phytomedicine 71, 153240.

R. B. Gupta and J.-J. Shim, 2006. Solubility in supercritical carbon dioxide. CRC press.

A. B. Hendrich, 2006. Flavonoid‐membrane interactions: possible consequences for biological effects of some polyphenolic compounds 1. Acta Pharmacologica Sinica 27, 27-40.

I. Irina, C. Leila and G. Mohamed, 2020. Effect of Heat Treatment and Light Exposure on the Antioxidant Activity of Flavonoids Processes 8, 163-174.

W. Kaialy, 2016. A review of factors affecting electrostatic charging of pharmaceuticals and adhesive mixtures for inhalation. International journal of pharmaceutics 503, 262-276.

M. Kalani and R. Yunus, 2011. Application of supercritical antisolvent method in drug encapsulation: a review. International journal of nanomedicine 6, 1429.

M.-S. Kim, H.-S. Song, H. J. Park and S.-J. Hwang, 2012. Effect of solvent type on the nanoparticle formation of atorvastatin calcium by the supercritical antisolvent process. Chemical Pharmaceutical Bulletin 60, 543-547.

Q. Li, D. Huang, T. Lu, J. P. K. Seville, L. Xing and G. A. Leeke, 2017. Supercritical fluid coating of API on excipient enhances drug release. Chemical Engineering Journal 313, 317-327.

Y. Li, D.-J. Yang, S.-L. Chen, S.-B. Chen and A. S.-C. Chan, 2008. Process parameters and morphology in puerarin, phospholipids and their complex microparticles generation by supercritical antisolvent precipitation. International journal of pharmaceutics 359, 35-45.

G. Liu, H. Wang and Y. Jiang, 2013. Recrystallization and micronization of camptothecin by the supercritical antisolvent process: influence of solvents. Industrial Engineering Chemistry Research 52, 15049-15056.

V. Martín, R. Romero-Díez, S. Rodríguez-Rojo and M. J. Cocero, 2015. Titanium dioxide nanoparticle coating in fluidized bed via supercritical anti-solvent process (SAS). Chemical Engineering Journal 279, 425-432.

R. L. Matos, T. Lu, C. McConville, G. Leeke and A. Ingram, 2018. Analysis of curcumin precipitation and coating on lactose by the integrated supercritical antisolvent-fluidized bed process. The Journal of Supercritical Fluids 141, 143-156.

T. McGarry, M. Biniecka, D. J. Veale and U. Fearon, 2018. Hypoxia, oxidative stress and inflammation. Free Radical Biology and Medicine 125, 15-24.
H. Miao, Z. Chen, W. Xu, W. Wang, Y. Song and Z. Wang, 2018. Preparation and characterization of naringenin microparticles via a supercritical anti-solvent process. The Journal of Supercritical Fluids 131, 19-25.
A. Montes, L. Wehner, C. Pereyra and E. M. De La Ossa, 2016. Precipitation of submicron particles of rutin using supercritical antisolvent process. The Journal of Supercritical Fluids 118, 1-10.
A. Naeem, Y. Ming, H. Pengyi, K. Y. Jie, L. Yali, Z. Haiyan, X. Shuai, L. Wenjing, W. Ling and Z. M. Xia, 2021. The fate of flavonoids after oral administration: a comprehensive overview of its bioavailability. Critical Reviews in Food Science and Nutrition, 1-18.
R. L. Nagula and S. Wairkar, 2019. Recent advances in topical delivery of flavonoids: A review. Journal of controlled release 296, 190-201.
W.-h. Niu, F. Wu, W.-y. Cao, Z.-g. Wu, Y.-C. Chao, F. Peng and C. Liang, 2021. Network pharmacology for the identification of phytochemicals in traditional Chinese medicine for COVID-19 that may regulate interleukin-6. Bioscience Reports 41.
C. Ober, 2013. title.
C. A. Ober, L. Kalombo, H. Swai and R. B. Gupta, 2013. Preparation of rifampicin/lactose microparticle composites by a supercritical antisolvent-drug excipient mixing technique for inhalation delivery. Powder technology 236, 132-138.
G. Ozkan, P. Franco, E. Capanoglu and I. De Marco, 2019. PVP/flavonoid coprecipitation by supercritical antisolvent process. Chemical Engineering Processing-Process Intensification 146, 107689.
L. Padrela, M. A. Rodrigues, A. Duarte, A. M. A. Dias, M. E. M. Braga and H. C. d. Sousa, 2018. Supercritical carbon dioxide-based technologies for the production of drug nanoparticles/nanocrystals – A comprehensive review. Advanced Drug Delivery Reviews 131, 22-78.
A. N. Panche, A. D. Diwan and S. R. Chandra, 2016. Flavonoids: an overview. Journal of nutritional science 5.
D. Prochazkova, I. Bousova and N. Wilhelmova, 2011. Antioxidant and prooxidant properties of flavonoids. Fitoterapia 82, 513-523.
E. Reverchon, I. De Marco and E. Torino, 2007. Nanoparticles production by supercritical antisolvent precipitation: a general interpretation. The Journal of Supercritical Fluids 43, 126-138.
M. T. M. Rosa, V. H. Alvarez, J. Q. Albarelli, D. T. Santos, M. A. A. Meireles and M. D. Saldana, 2020. Supercritical anti-solvent process as an alternative technology for vitamin complex encapsulation using zein as wall material: Technical-economic evaluation. The Journal of Supercritical Fluids 159, 104499.
J. A. Ross and C. M. Kasum, 2002. Dietary flavonoids: bioavailability, metabolic effects, and safety. Annual review of Nutrition 22, 19-34.
M. Rossmann, A. Braeuer and E. Schluecker, 2014. Supercritical antisolvent micronization of PVP and ibuprofen sodium towards tailored solid dispersions. The Journal of Supercritical Fluids 89, 16-27.
G. Saint-Lorant, P. Leterme, A. Gayot and M. Flament, 2007. Influence of carrier on the performance of dry powder inhalers. International journal of pharmaceutics 334, 85-91.
K. T. Savjani, A. K. Gajjar and J. K. Savjani, 2012. Drug solubility: importance and enhancement techniques. International Scholarly Research Notices 2012, 1-10.
F. Sheng, P. S. Chow, J. Hu, S. Cheng, L. Guo and Y. Dong, 2020. Preparation of quercetin nanorod/microcrystalline cellulose formulation via fluid bed coating crystallization for dissolution enhancement. International Journal of Pharmaceutics 576, 118983.
B. Sinha, R. H. Müller and J. P. Möschwitzer, 2013. Bottom-up approaches for preparing drug nanocrystals: formulations and factors affecting particle size. International journal of pharmaceutics 453, 126-141.
H. Steckel, J. Thies and B. Müller, 1997. Micronizing of steroids for pulmonary delivery by supercritical carbon dioxide.

International journal of pharmaceutics 152, 99-110.
X. Sui, W. Wei, L. Yang, Y. Zu, C. Zhao, L. Zhang, F. Yang and Z. Zhang, 2012. Preparation, characterization and in vivo assessment of the bioavailability of glycyrrhizic acid microparticles by supercritical anti-solvent process. International journal of pharmaceutics 423, 471-479.
I. Trujillo-Mayol, M. Guerra-Valle, N. Casas-Forero, M. M. C. Sobral, O. Viegas, J. Alarcon-Enos, I. M. P. L. V. O. Ferreira and O. Pinho, 2021. Western Dietary Pattern Antioxidant Intakes and Oxidative Stress: Importance During the SARS-CoV-2/COVID-19 Pandemic. Advances in Nutrition 12, 670-681.
P. Varughese, J. Li, W. Wang and D. Winstead, 2010. Supercritical antisolvent processing of γ-Indomethacin: Effects of solvent, concentration, pressure and temperature on SAS processed Indomethacin. Powder Technology 201, 64-69.
J.-Z. Wang, R.-Y. Zhang and J. Bai, 2020. An anti-oxidative therapy for ameliorating cardiac injuries of critically ill COVID-19-infected patients. International Journal of Cardiology 312, 137-138.
F. Xia, D. Hu, H. Jin, Y. Zhao and J. Liang, 2012. Preparation of lutein proliposomes by supercritical anti-solvent technique. Food hydrocolloids 26, 456-463.
Q.-D. Xia, Y. Xun, J.-L. Lu, Y.-C. Lu, Y.-Y. Yang, P. Zhou, J. Hu, C. Li and S.-G. Wang, 2020. Network pharmacology and molecular docking analyses on Lianhua Qingwen capsule indicate Akt1 is a potential target to treat and prevent COVID-19. Cell Proliferation 53.
T. Xiao, Y. Wei, M. Cui, X. Li, H. Ruan, L. Zhang, J. Bao, S. Ren, D. Gao, M. Wang, R. Sun, M. Li, J. Lin, D. Li, C. Yang and H. Zhou, 2021. Effect of dihydromyricetin on SARS-CoV-2 viral replication and pulmonary inflammation and fibrosis. Phytomedicine 91.
H. Yan and C. Zou, 2021. Mechanism and material basis of LianhuaQingwen capsule for improving clinical cure rate of COVID-19: a study based on network pharmacology and molecular docking technology. Nan fang yi ke da xue xue bao = Journal of Southern Medical University 41, 20-30.
S.-D. Yeo and E. Kiran, 2005. Formation of polymer particles with supercritical fluids: A review. The Journal of Supercritical Fluids 34, 287-308.

Figure 1

a.

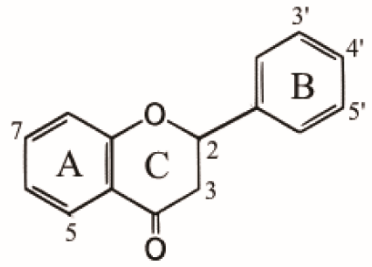

	3	5	7	3’	4’	5’	C_2-C_3
LUT	-	-OH	-OH	-OH	-OH	-	C=C
NRG	-	-OH	-OH	-	-OH	-	C-C
DMY	-OH	-OH	-OH	-OH	-OH	-OH	C-C

b.

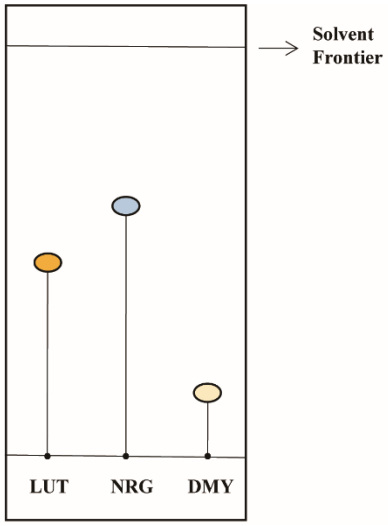

Fig. 1. Structures and properties of three flavonoids (a) and the polarity of three flavonoids was determined by silica gel thin layer method (b).

Figure 2

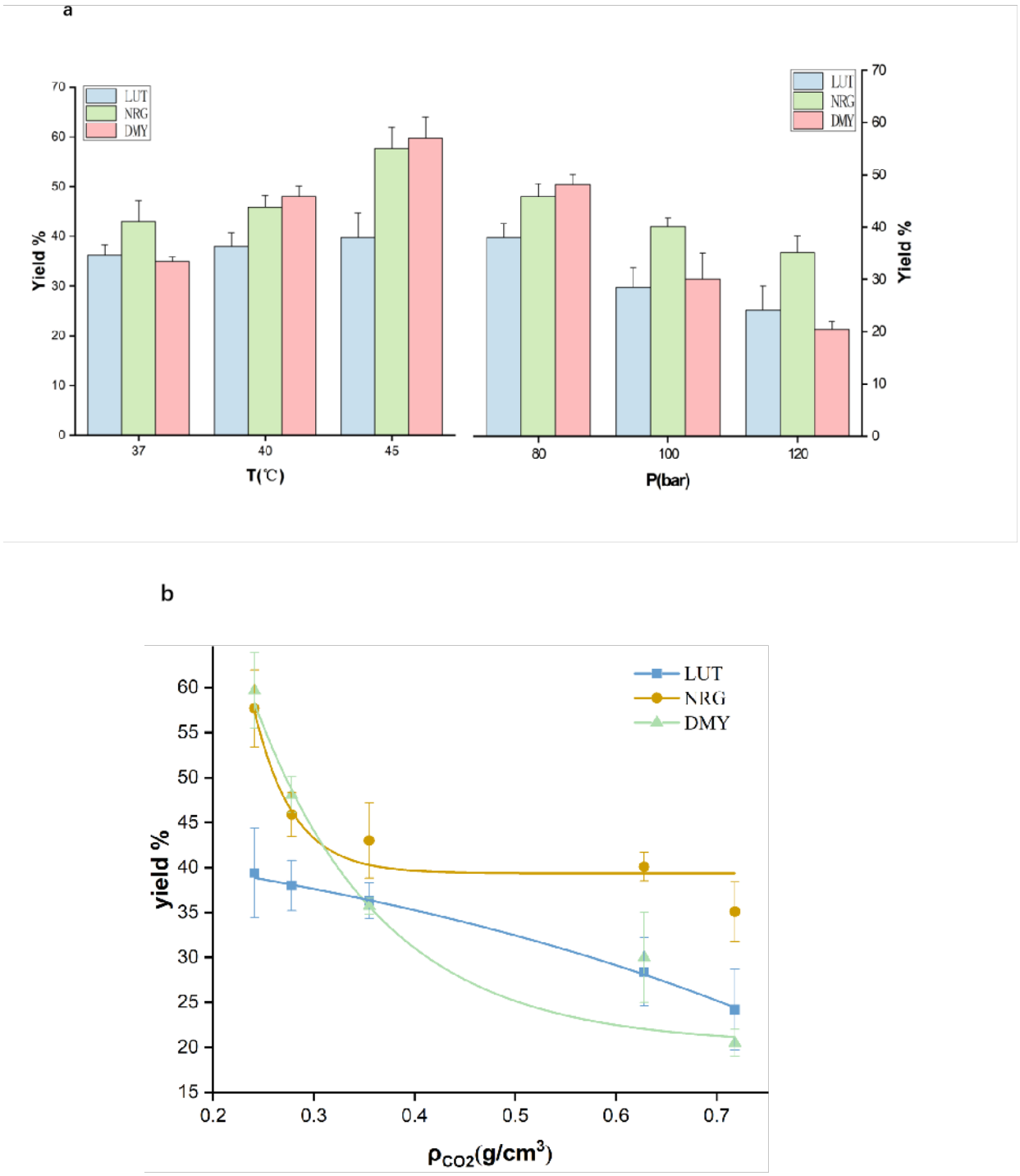

Fig. 2. Effect of temperature and pressure on yield. (a) Histogram of yield at different temperature and pressure; (b) Relationship between sc-CO2 density and yield.

Figure 3

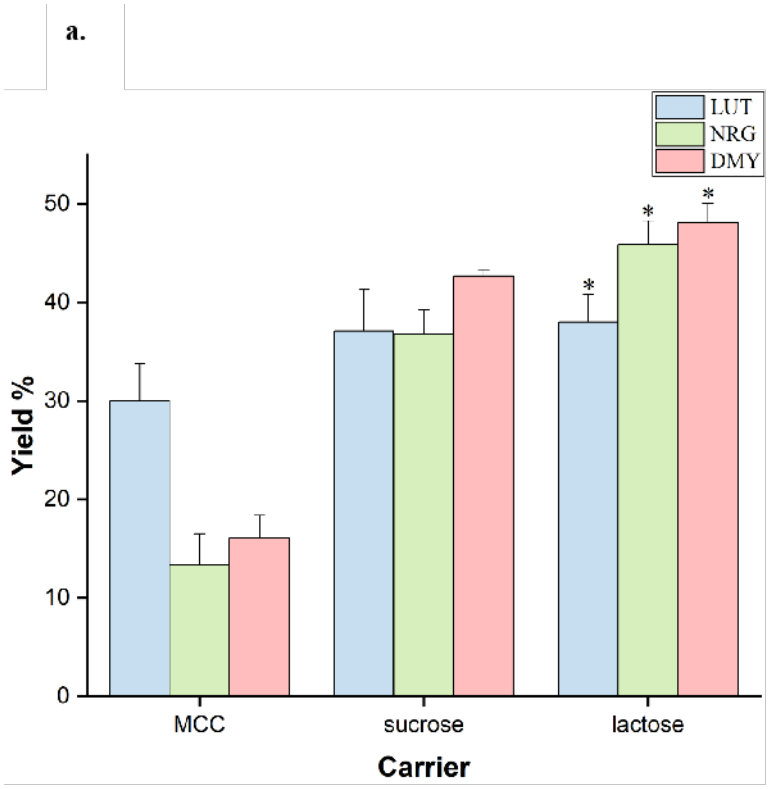
a.
LUT
NRG
DMY
Yield %
0
10
20
30
40
50
*
*
*
MCC
sucrose
lactose
Carrier

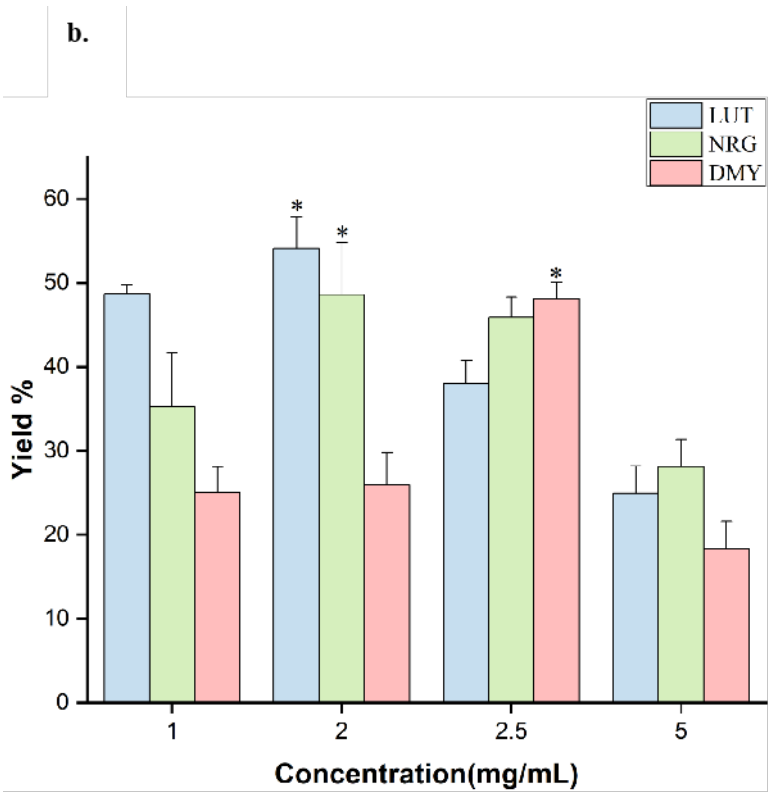
b.
LUT
NRG
DMY
Yield %
0
10
20
30
40
50
60
*
*
*
1
2
2.5
5
Concentration(mg/mL)

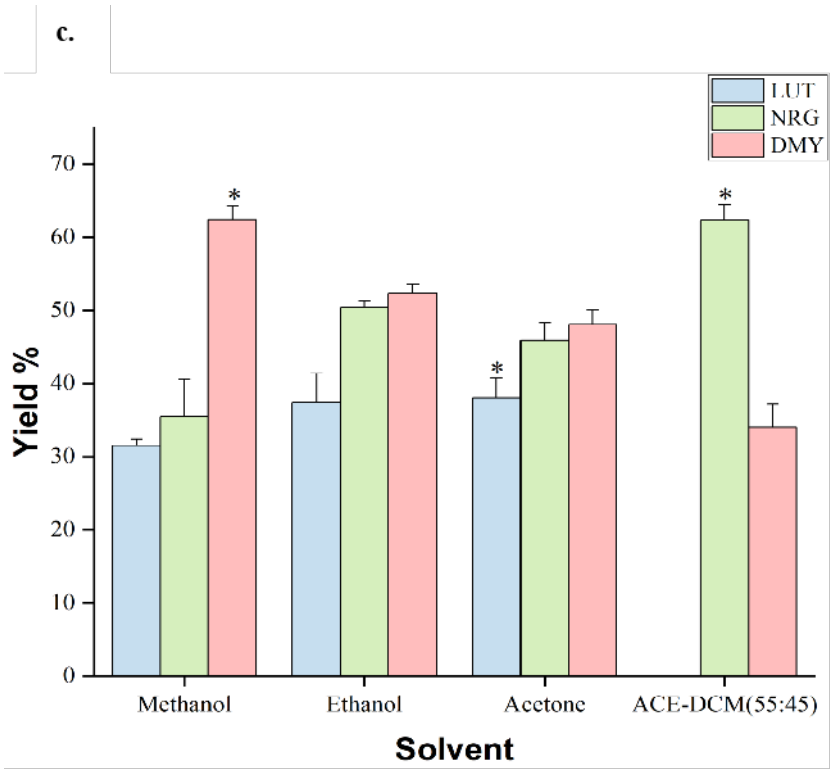

Fig. 3. Effect of different parameters on yield: (a) Carrier; (b) Concentration and (c) Solvent. (* means the highest yield at this parameters)

Figure 4

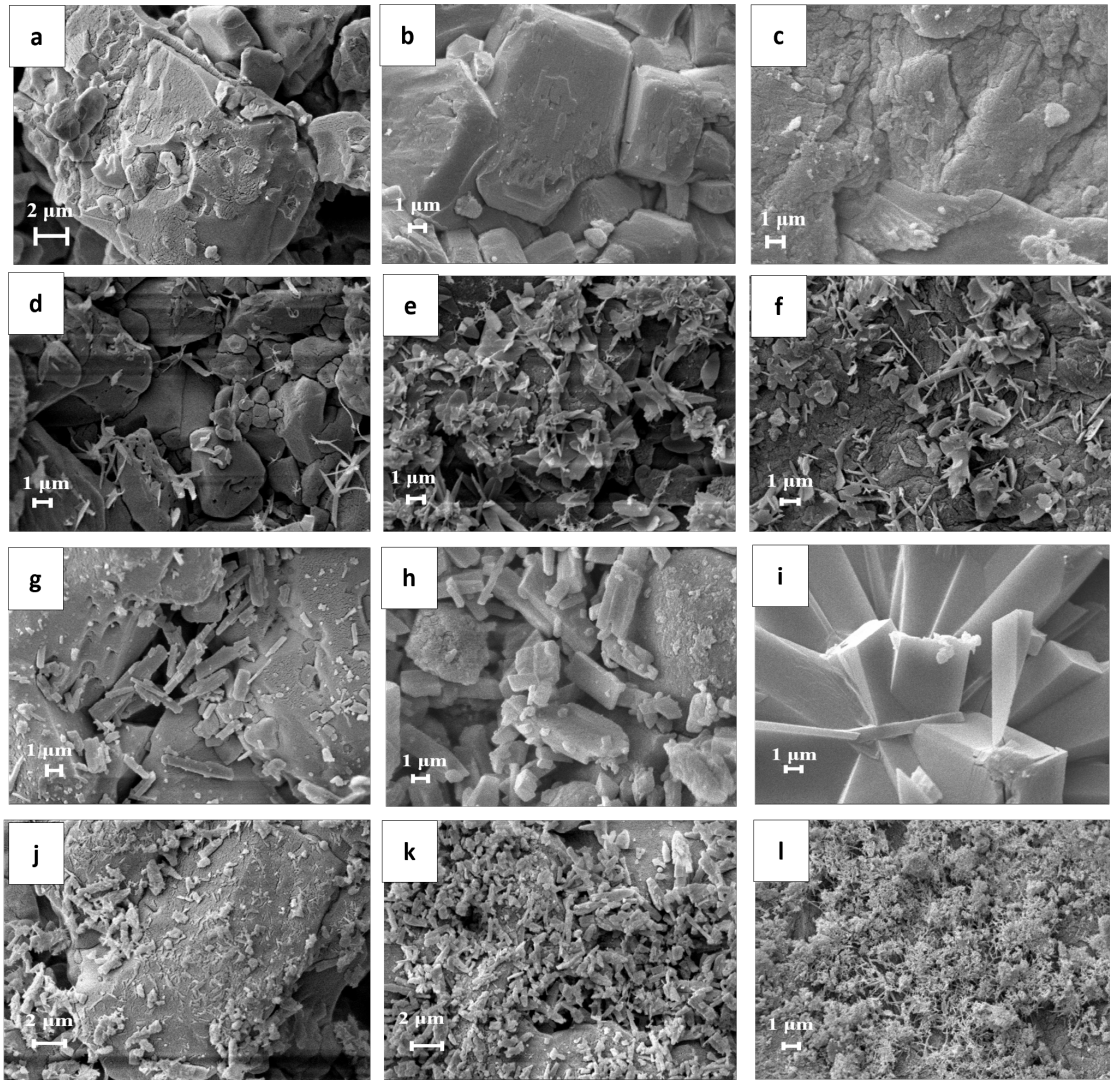

Fig. 4. The scanning electron microscopy images of uncoated carriers; LUT/NRG/DMY SAS-FB samples prepared with different carriers. (a) Uncoated lactose x 5000; (b) Uncoated sucrose x 5000; (c) Uncoated MCC x 5000; (d) SAS-FB samples of LUT on lactose x 5000; (e) SAS-FB samples of LUT on sucrose x 5000; (f) SAS-FB samples of LUT on MCC 5000; (g) SAS-FB samples of NRG on lactose x 5000; (h) SAS-FB samples of NRG on sucrose x 5000; (i) SAS-FB samples of NRG on MCC x 5000; (j) SAS-FB samples of DMY on lactose x 5000; (k) SAS-FB samples of DMY on sucrose x 5000; (l) SAS-FB samples of DMY on MCC x 5000.

Figure 5

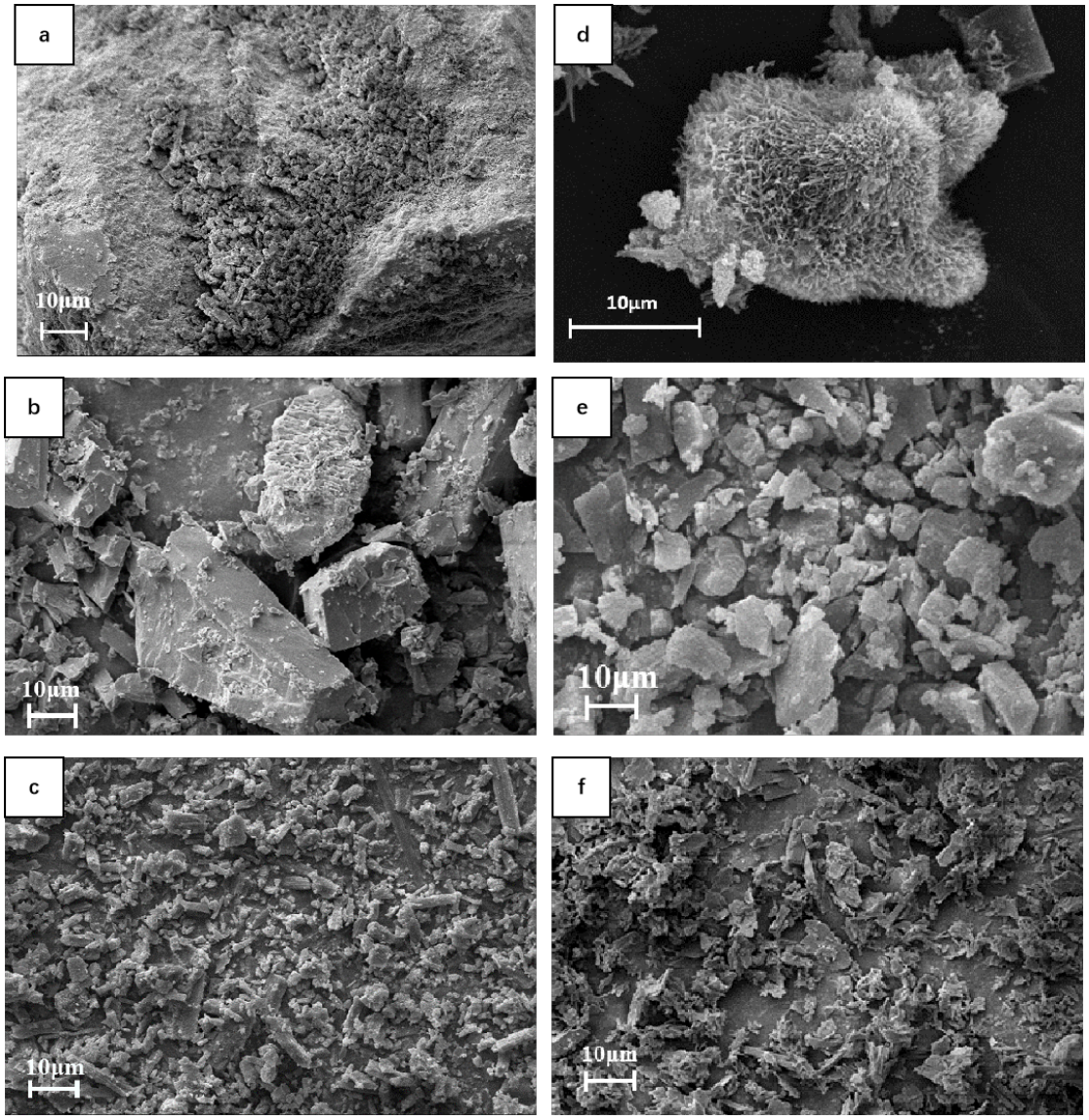

Fig. 5. The scanning electron microscopy images of unprocessed flavonoids and SAS samples. (a) uprocessed LUT x 1000; (b) uprocessed NRG x 1000; (c) uprocessed DMY x 1000; (d) LUT-SAS sample x 2500; (e) NRG-SAS sample x 1000; (f) DMY-SAS sample x 1000.

Figure 6

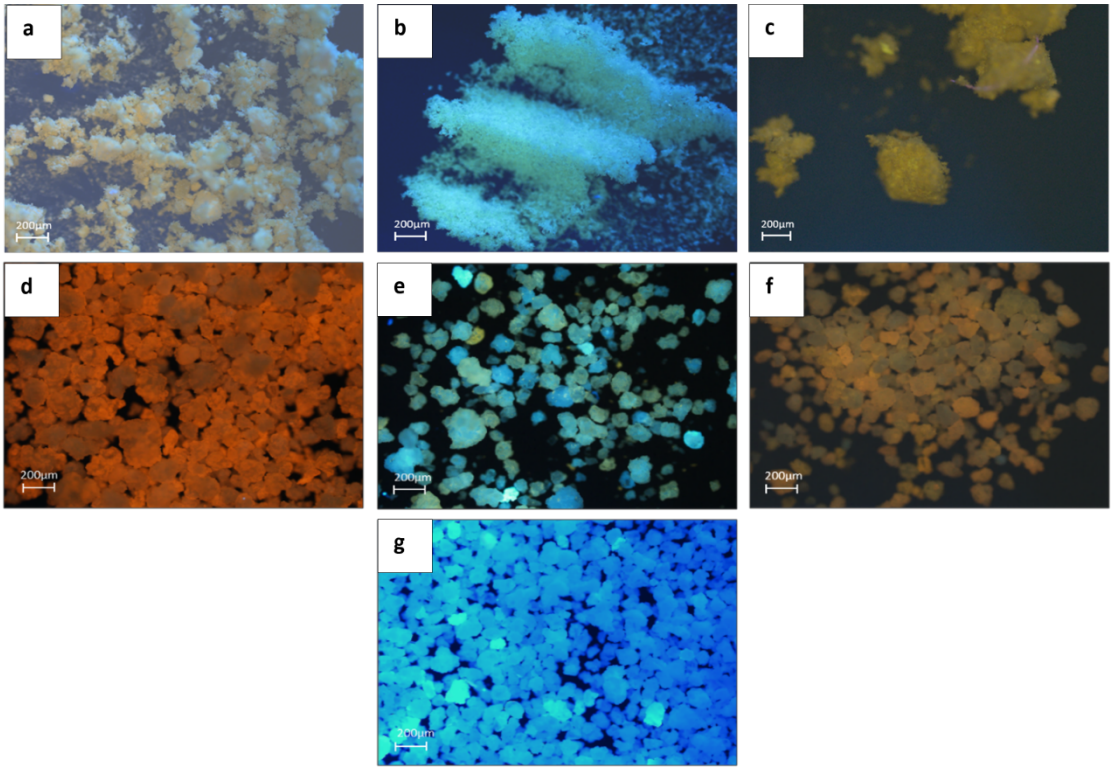

Fig. 6. Fluorescence microscopy of (a) unprocessed LUT, (b) unprocessed NRG, (c) unprocessed DMY, (d) SAS-FB samples of LUT, (e) SAS-FB samples of NRG, (f) SAS-FB samples of DMY and (g) uncoated lactose.

Figure 7

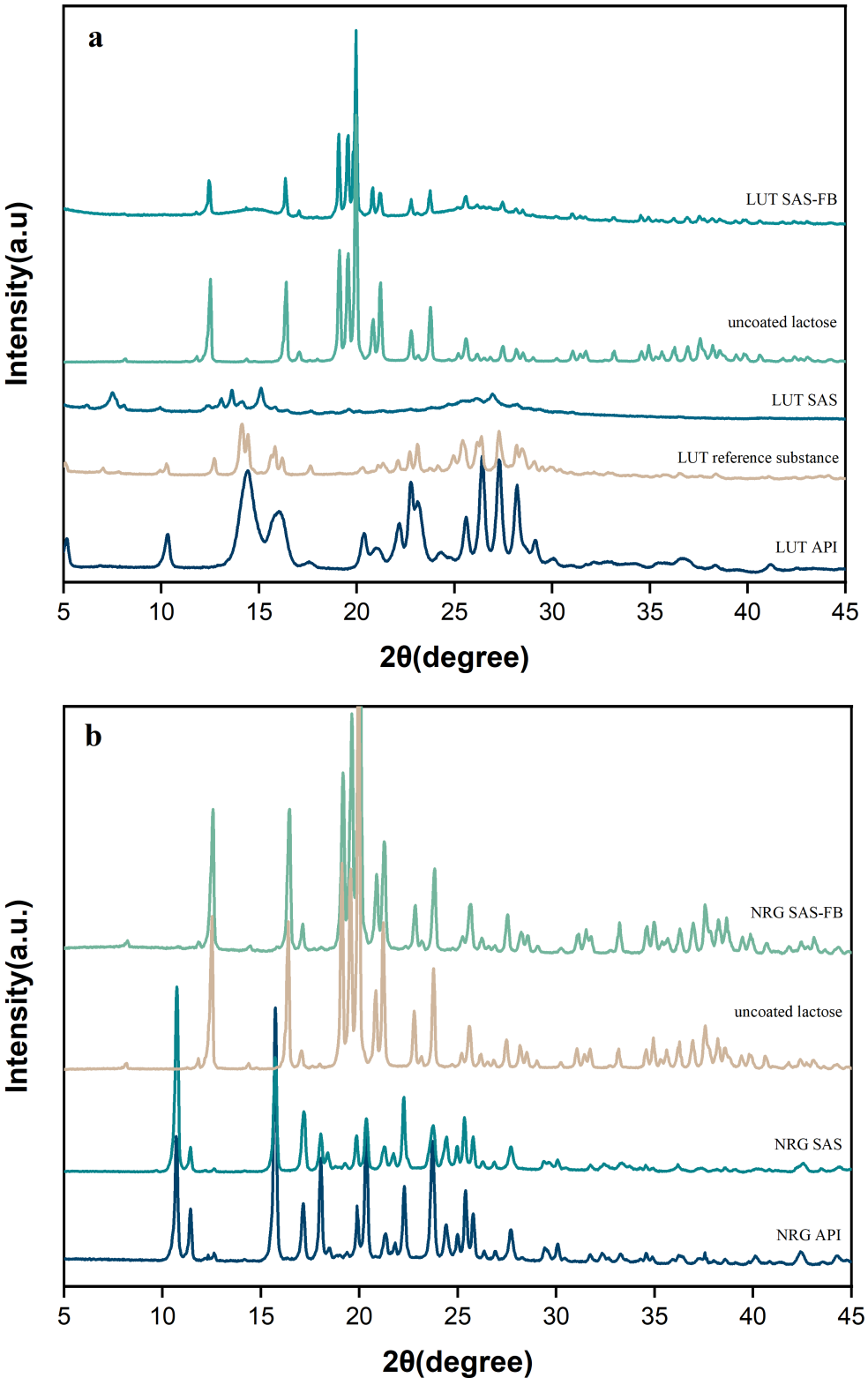
a
LUT SAS-FB
uncoated lactose
LUT SAS
LUT reference substance
LUT API
Intensity(a.u)
5
10
15
20
25
30
35
40
45
2θ(degree)
b
NRG SAS-FB
uncoated lactose
NRG SAS
NRG API
Intensity(a.u.)
5
10
15
20
25
30
35
40
45
2θ(degree)

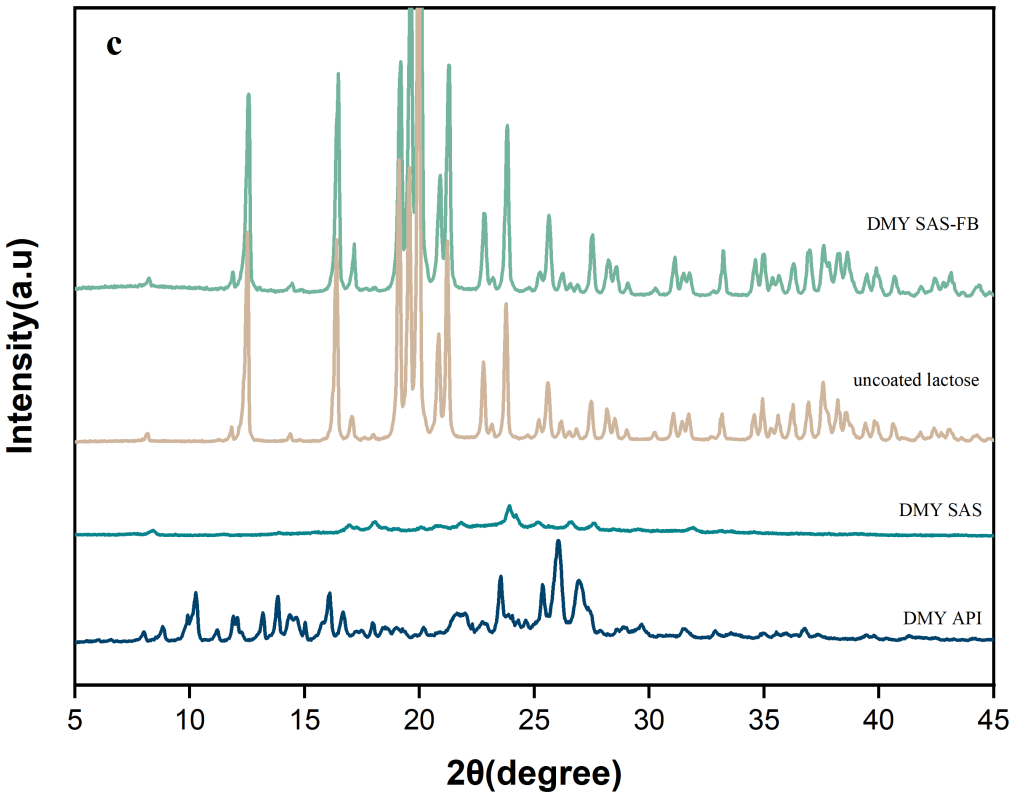

Fig. 7. X-Ray Powder Diffraction patterns of (a) LUT SAS-FB, uncoated lactose, LUT SAS samples, LUT reference substance and LUT API; (b) NRG SAS-FB, uncoated lactose, NRG SAS samples and NRG API; (c) DMY SAS-FB, uncoated lactose, DMY SAS samples and DMY API.

Figure 8

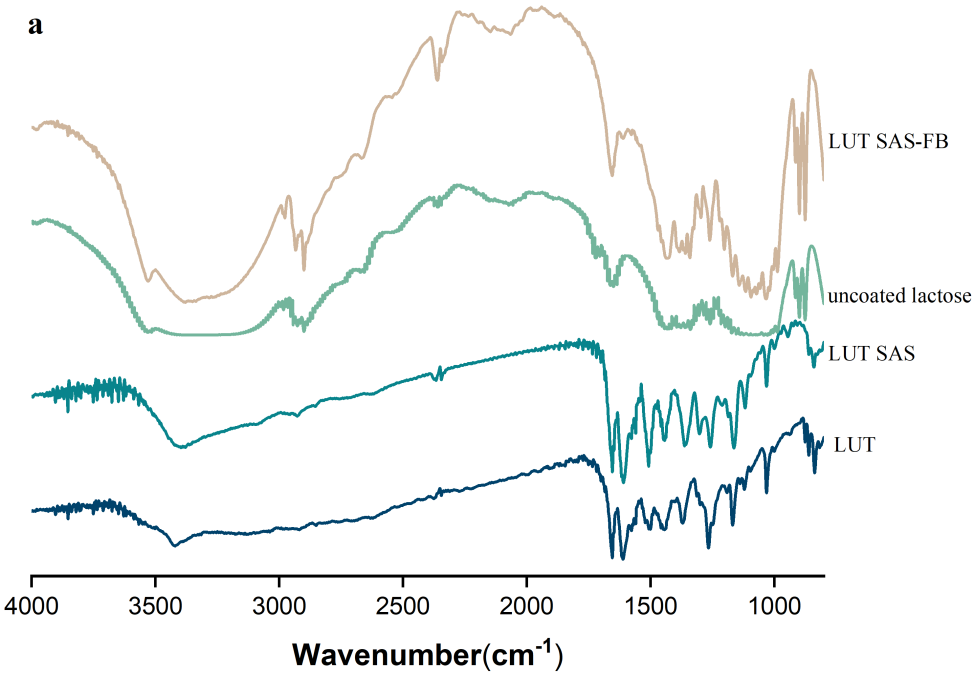
a
LUT SAS-FB
uncoated lactose
LUT SAS
LUT
4000
3500
3000
2500
2000
1500
1000
Wavenumber(cm-1)

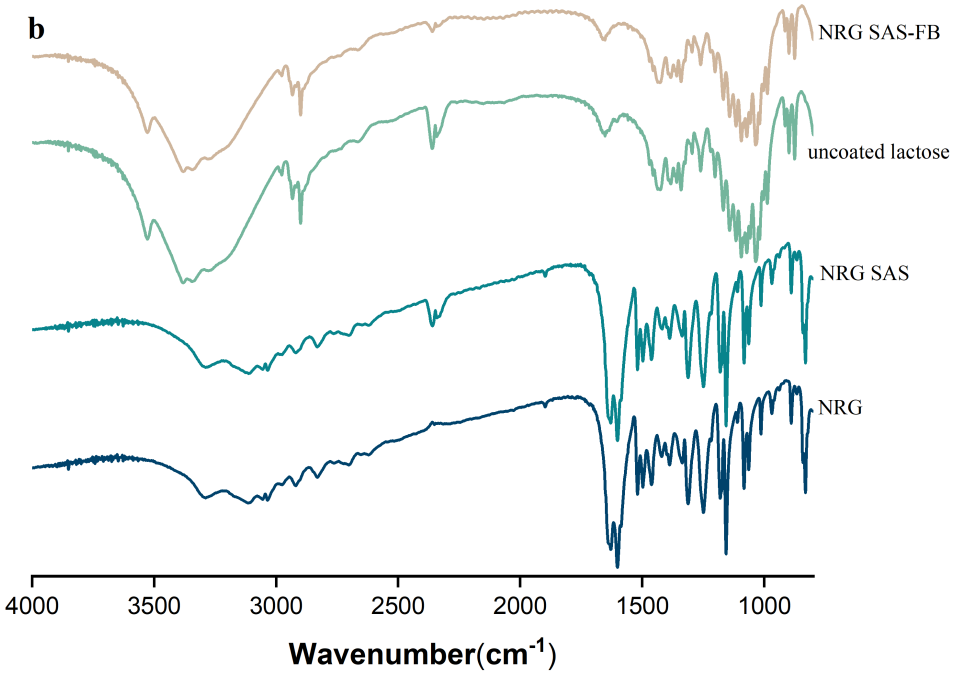
b
NRG SAS-FB
uncoated lactose
NRG SAS
NRG
4000
3500
3000
2500
2000
1500
1000
Wavenumber(cm-1)

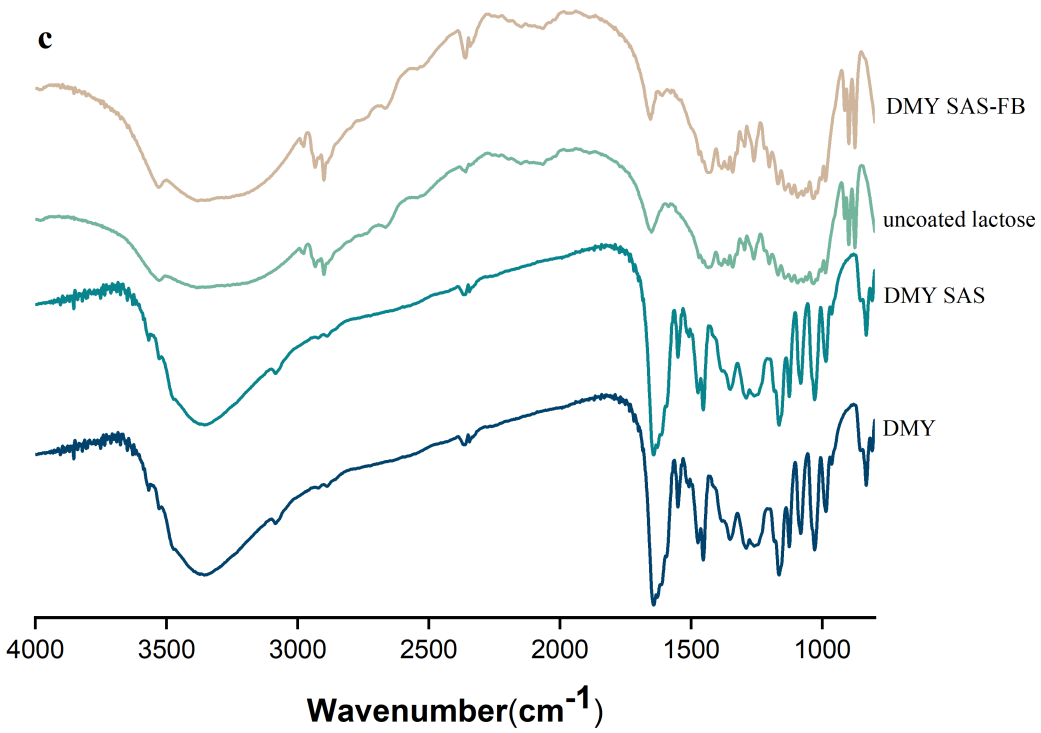

Fig. 8. Fourier transform infrared spectroscopy spectra of (a) LUT SAS-FB samples, lactose, LUT SAS samples and LUT; (b) NRG SAS-FB samples, lactose, NRG SAS samples and NRG; (c) DMY SAS-FB samples, lactose, DMY SAS samples and DMY.

Figure 9

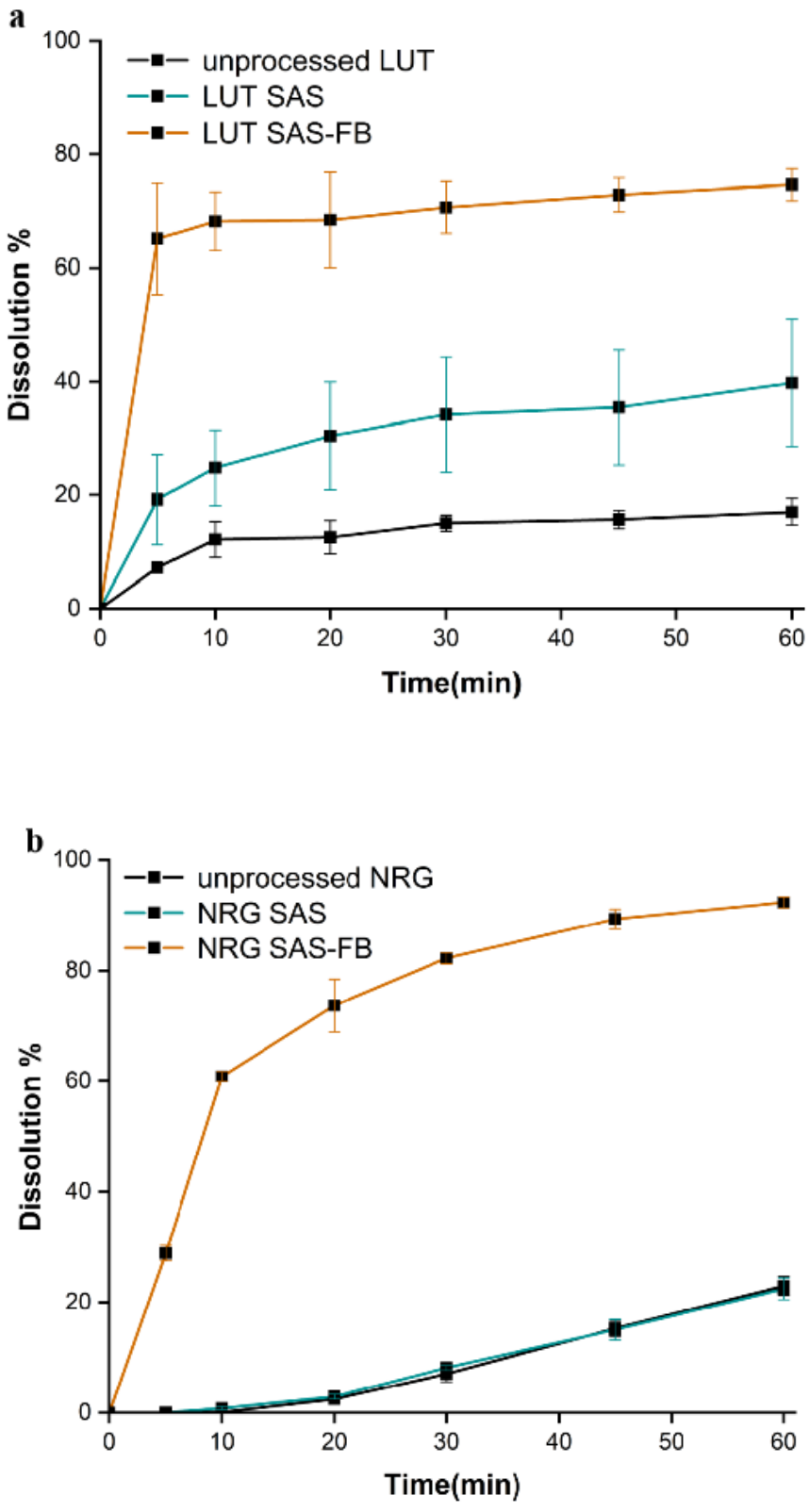
a
unprocessed LUT
LUT SAS
LUT SAS-FB
Dissolution %
Time(min)
0
20
40
60
80
100
0
10
20
30
40
50
60
b
unprocessed NRG
NRG SAS
NRG SAS-FB
Dissolution %
Time(min)

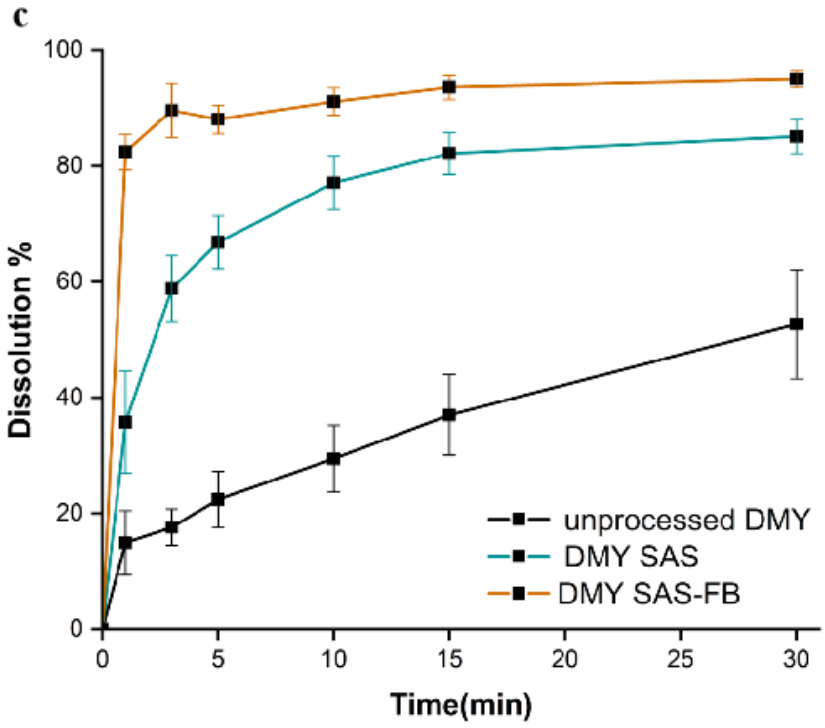

Fig. 9. (a) The dissolution profile of unprocessed LUT, SAS and SAS-FB particles; (b) the dissolution profile of unprocessed NRG, SAS and SAS-FB particles; (c) the dissolution profile of unprocessed DMY, SAS and SAS-FB particles.

Figure 10

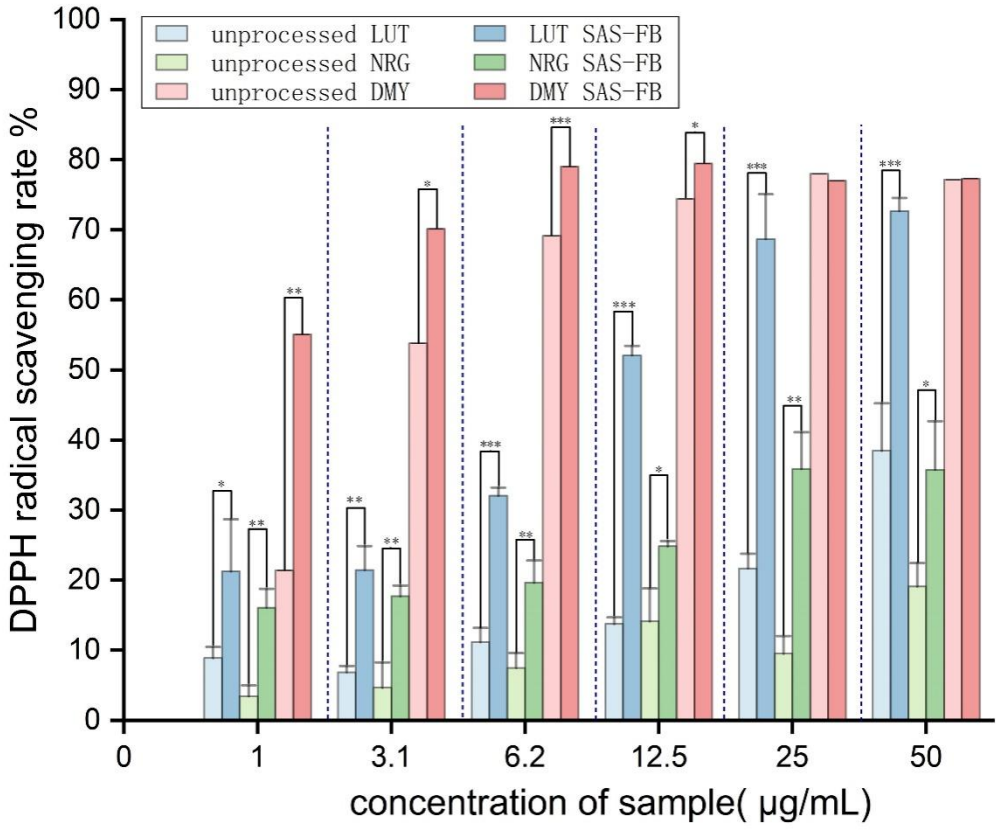

Fig. 10. 1,1-diphenyl-2-dinitrophenylhydrazine (DPPH) radical-scavenging activity of the unprocessed flavonoids and SAS-FB (* $P < 0.05$, ** $P < 0.01$, *** $P < 0.001$).

Supercritical fluid coating of flavonoids on excipients enhances drug release and antioxidant activity

(Supplementary Information)

Hongling He,[a,∇] Yating Huang,[a,∇] Xiubing Zhang,[b,∇] Yanting Ouyang,[c,∇] Piaopiao Pan[d], yanling Lan,[a] Zicheng Zhong,[a] Lu Ping,[b] Tiejun Lu,[e] Zhenqiu Chen,[b,*] Lei Xing,[f,*] Qingguo Li,[a,*] Zhenwen Qiu,[b,*]

[a] School of Pharmaceutical Sciences, Guangzhou University of Chinese Medicine, Guangzhou 510006, P.R. China

[b] The First Affiliated Hospital, Guangzhou University of Chinese Medicine, Guangzhou 510405, P.R. China

[c] Shunde Hospital of Guangzhou University of Chinese Medicine, Foshan 528329, Guangdong, P.R. China

[d] Institute of Infection, Immunity and Inflammation, University of Glasgow, Glasgow G12 8QQ, UK

[e] Centre for Formulation Engineering, School of Chemical Engineering, University of Birmingham, Birmingham B15 2TT, UK

[f] Department of Chemical and Process Engineering, University of Surrey, Guildford GU2 7XH, UK

[∇] HH, YH, XZ, and YO contributed equally to this paper.

***Corresponding author**:

Zhenwen Qiu, The First Affiliated Hospital, Guangzhou University of Chinese Medicine, E-mail: qzhenwen@gzucm.edu.cn

Qingguo Li, School of Pharmaceutical Sciences, Guangzhou University of Chinese Medicine, 232 University City Ring Road East, Panyu District, Guangzhou 510006, China, E-mail: lqg8512@gzucm.edu.cn

Lei Xing, Department of Chemical and Process Engineering, Faculty of Engineering and Physical Sciences, University of Surrey, Guildford GU2 7XH, UK, E-mail: l.xing@surrey.ac.uk

Zhenqiu Chen, The First Affiliated Hospital, Guangzhou University of Chinese Medicine, E-mail: chenzhenqiu2012@126.com

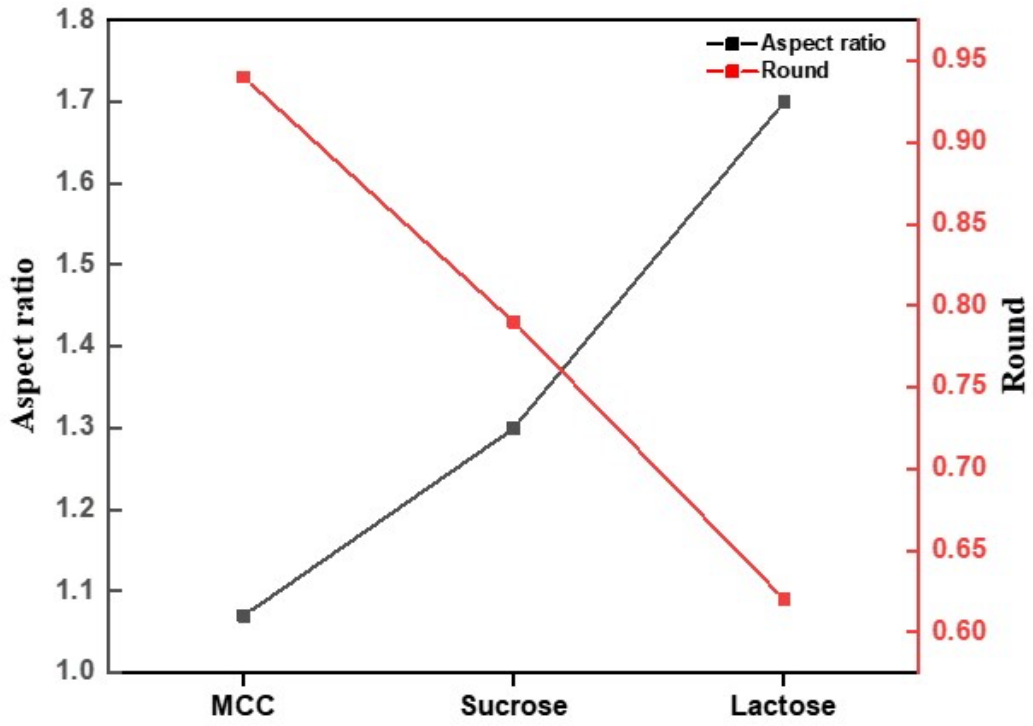

Fig. S1. Aspect ratio and round of carrier (Aspect ratio and round values close to 1.0 indicate better particle roundness).

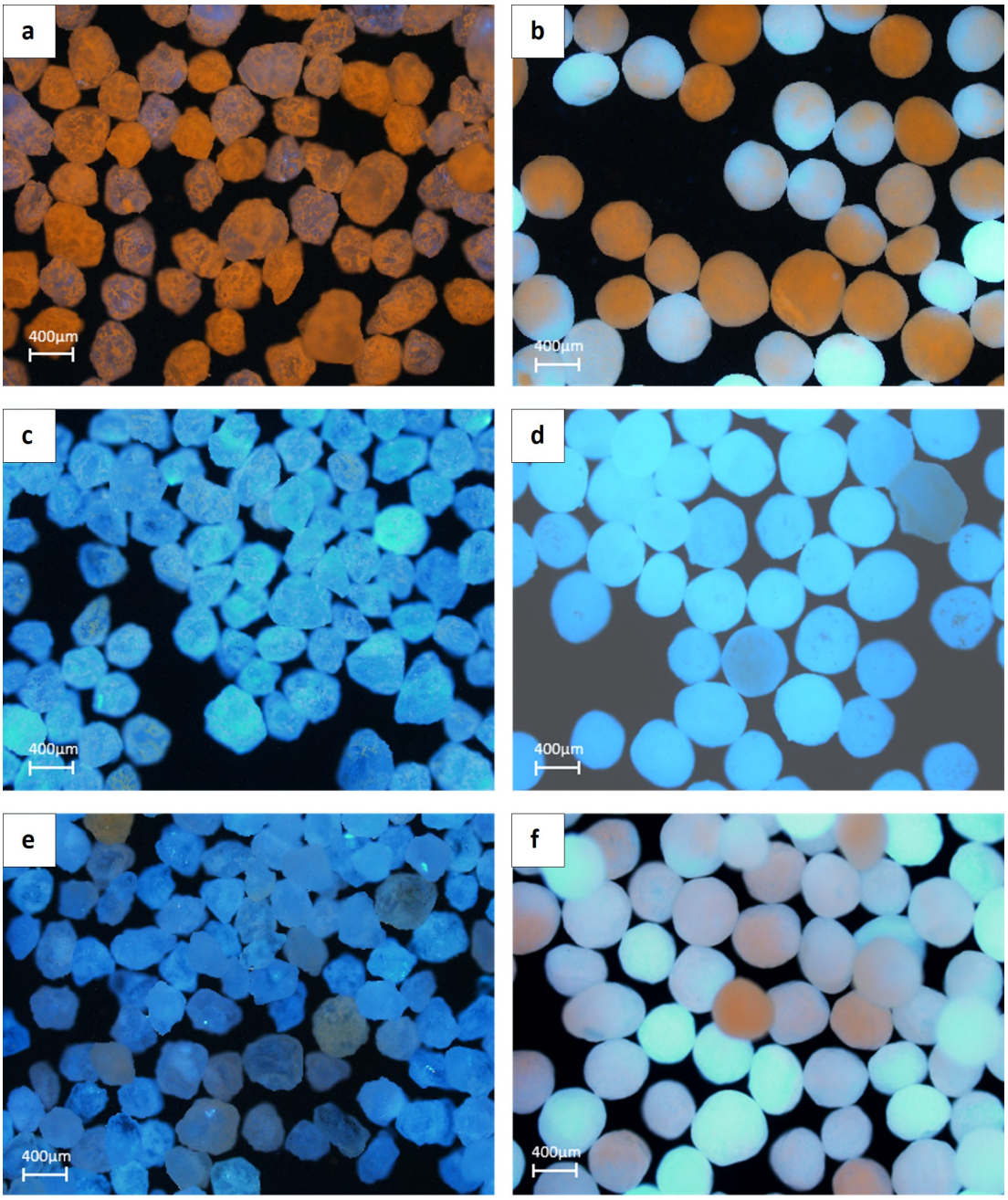

Fig. S2. Fluorescence microscopy of SAS-FB samples of LUT coated on sucrose (a) and MCC (b); SAS-FB samples of NRG on sucrose (c) and MCC (d) ; SAS-FB samples of DMY on sucrose (e) and MCC (f).

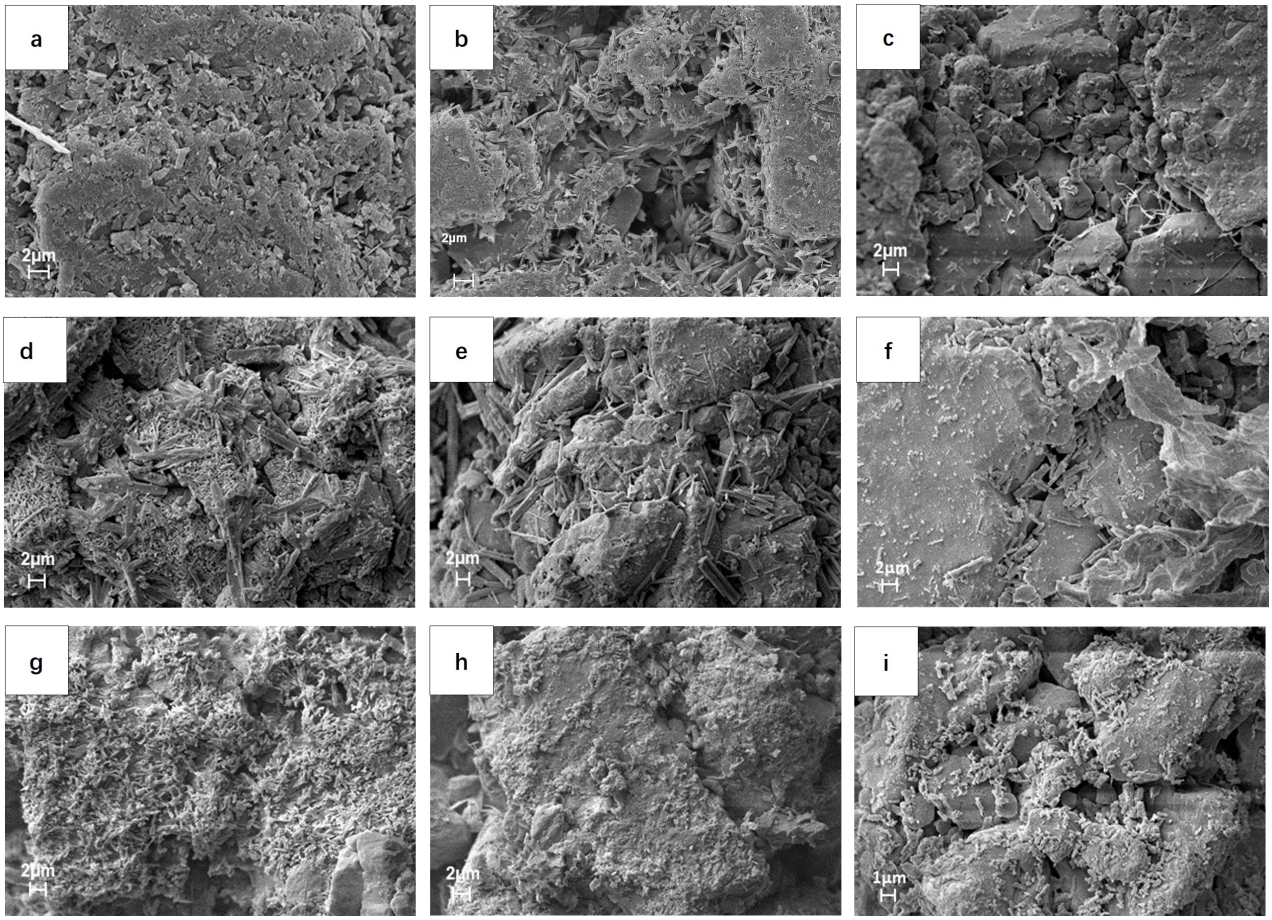

Fig. S3. The scanning electron microscopy images of flavonoids coated lactose particles at 80 bar and 40 ℃. Effect of solvents: (a) $LUT_{Methanol}$ x 2000; (b) $LUT_{Ethanol}$ x 2000; (c) $LUT_{Acetone}$ x 2000; (d) $NRG_{Methanol}$ x 2000; (e) $NRG_{Ethanol}$ x 2000; (f) $NRG_{Acetone}$ x 2000; (g) $DMY_{Methanol}$ x 2000; (h) $DMY_{Ethanol}$ x 2000; (i) $DMY_{Acetone}$ x 2000. Experimental conditions are detailed in Table 2.

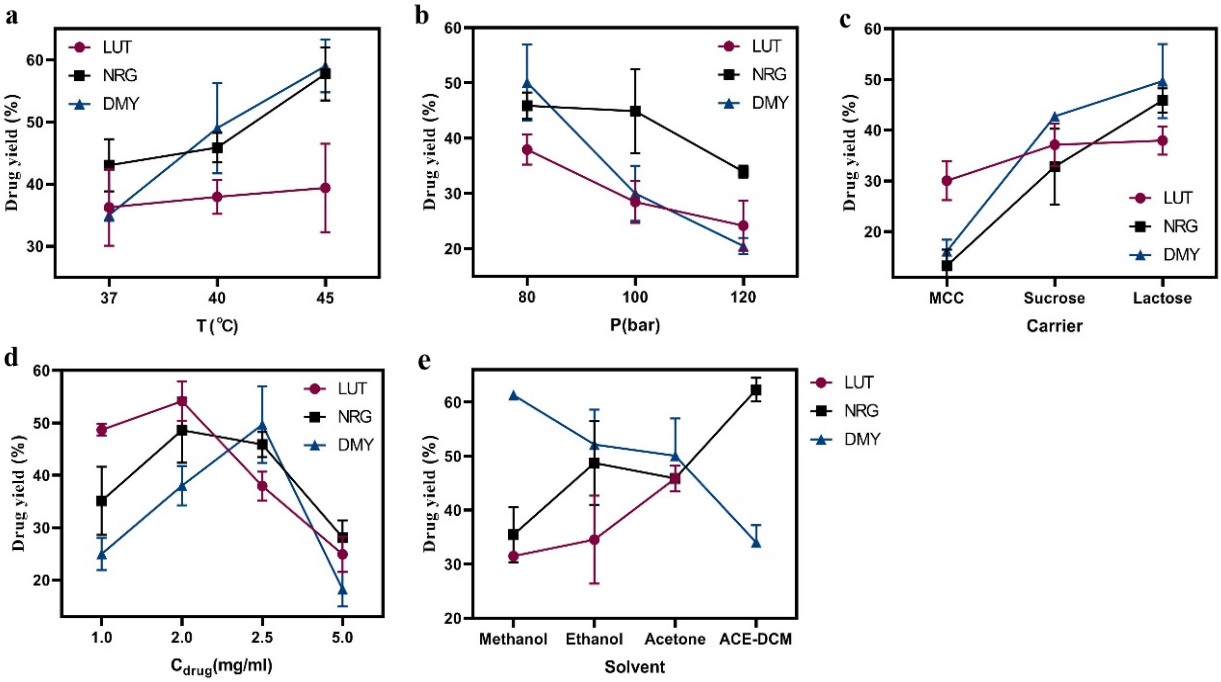

Fig. S4. Effects of process parameters on the yield of three flavonoids.

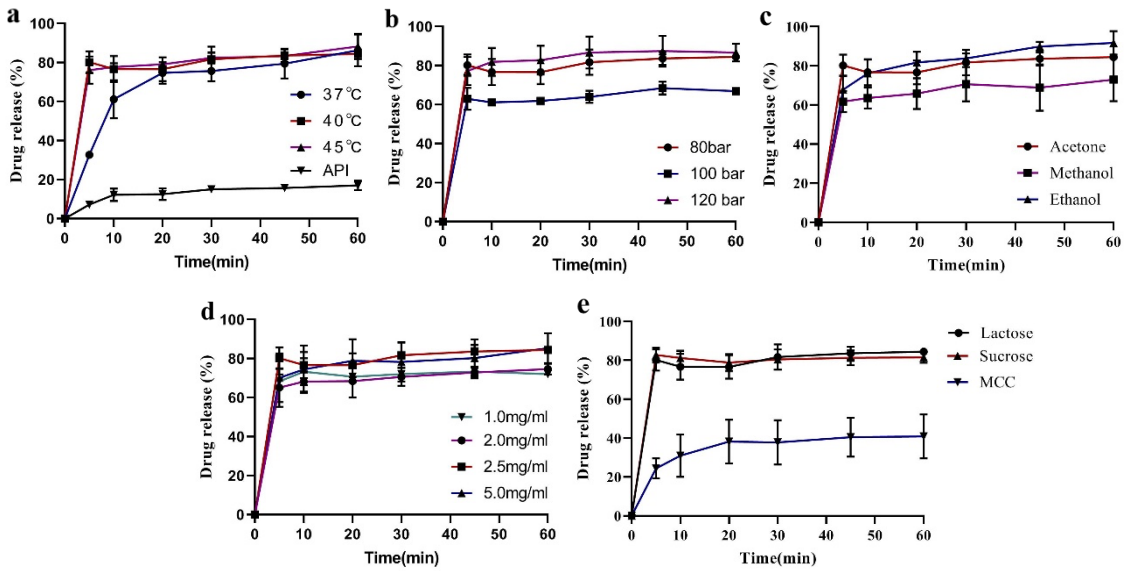

Fig. S5. Influence of LUT process parameters on drug dissolution. (a. the influence of temperature; b. the influence of pressure; c. Influence of liquid concentration; d. Influence of solvents; e. Influence of different carriers).

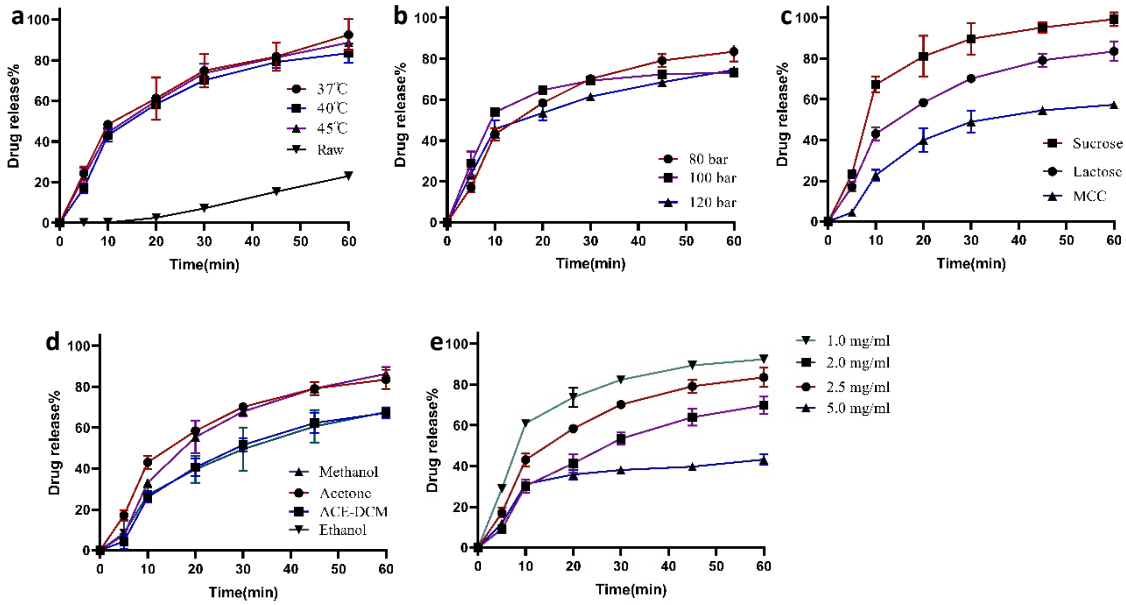

Fig. S6. Influence of NRG process parameters on drug dissolution. (a. the influence of temperature; b. the influence of pressure; c. Influence of different carriers; d. Influence of solvents; e. Influence of liquid concentration.)

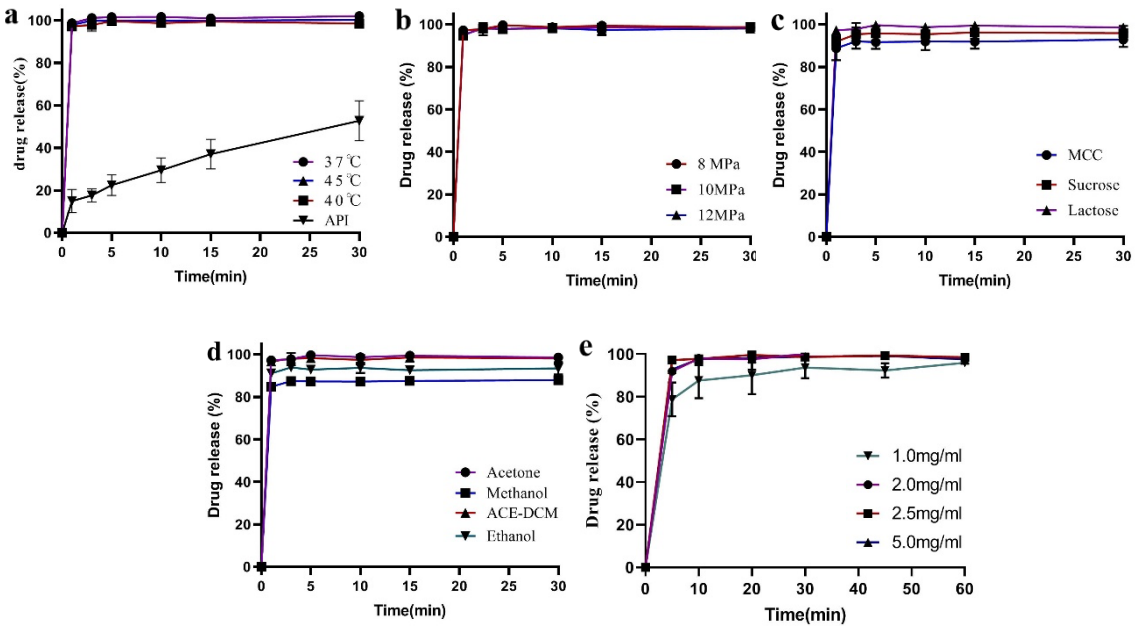

Fig. S7. Influence of DMY process parameters on drug dissolution. (a. the influence of temperature; b. the influence of pressure; c. Influence of different carriers; d. Influence of solvents; e. Influence of liquid concentration.)

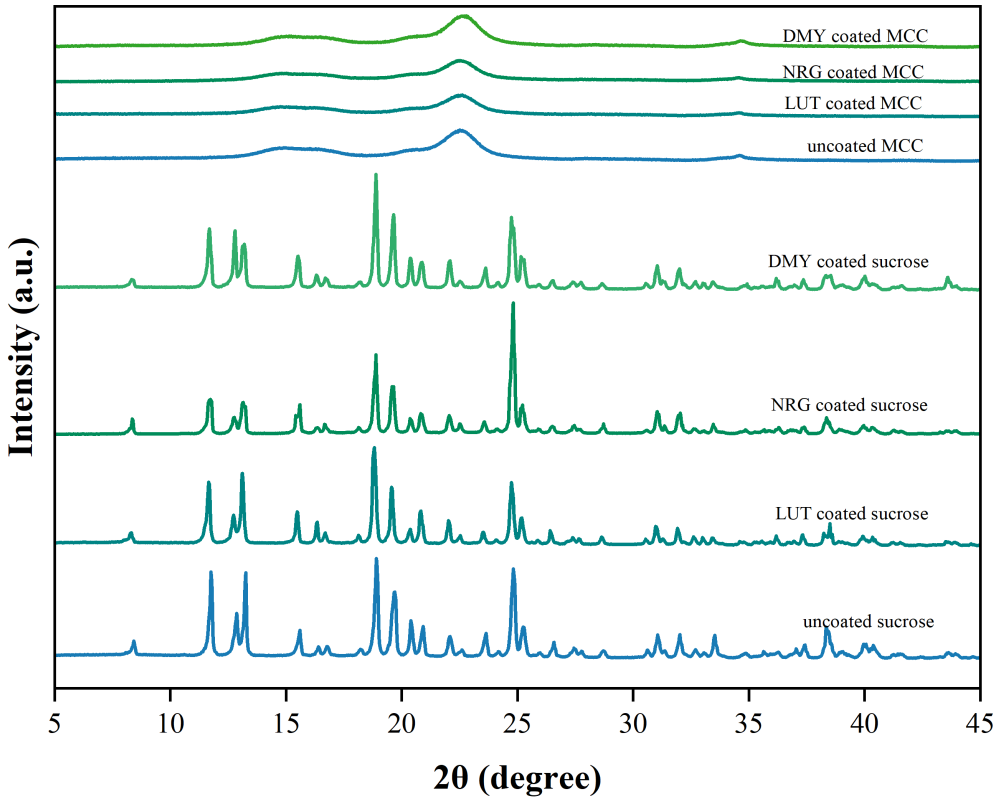

Fig. S8. X-Ray Powder Diffraction patterns of uncoated sucrose, uncoated MCC and corresponding SAS-FB samples of LUT, NRG and DMY.